1990

Enhanced selectivity and detectability in absorption and fluorescence methods based on polarization modulation

Patrice L. Christensen
Iowa State University

Order Number 9110489

Enhanced selectivity and detectability in absorption and fluorescence methods based on polarization modulation

Christensen, Patrice L., Ph.D.

Iowa State University, 1990

U·M·I
300 N. Zeeb Rd.
Ann Arbor, MI 48106

Enhanced selectivity and detectability in absorption and fluorescence methods based on polarization modulation

by

Patrice L. Christensen

A Dissertation Submitted to the
Graduate Faculty in Partial Fulfillment of the
Requirements for the Degree of
DOCTOR OF PHILOSOPHY

Department: Chemistry
Major: Analytical Chemistry

Approved:

Signature was redacted for privacy.

In Charge of Major Work

Signature was redacted for privacy.

For the Major Department

Signature was redacted for privacy.

For the Graduate College

Iowa State University
Ames, Iowa

1990

TABLE OF CONTENTS

CHAPTER I. INTRODUCTION TO OPTICAL POLARIZATION AND POLARIZATION MODULATION

Polarization is a fundamental property of light. While other properties of light such as color (wavelength or frequency) and intensity are more commonly considered in spectrochemical analysis, the polarization of light is often used to impart greater sensitivity or selectivity to a technique. A number of spectroscopic methods rely on polarized light and modulation of polarization. A list of techniques which fit into this category is given in Table 1. Several of these methods depend on inherent chirality (optical activity) in the molecules being probed. Optical rotatory dispersion (ORD) and circular dichroism (CD) are used extensively for analysis of natural optical activity. Other methods require the application of an external field to produce an optical anisotropy in an achiral sample. For example, the presence of a strong magnetic field produces anisotropies which can lead to the observation of magnetic optical rotatory dispersion (MORD) and magnetic circular dichroism (MCD) in systems which are not naturally optical active.

Description of Polarized Light

It is most convenient to describe light as a transverse wave when discussing polarization. Light is comprised of time-varying electric and magnetic fields. The fields can be described as vectors where E represents the electric vector and H represents the magnetic vector. Because these fields are perpendicular to one another and maintain a 90° phase difference along the propagation direction, it is common practice

Table 1. Selected spectroscopic methods which can utilize polarization modulation

Optical Rotatory Dispersion (ORD)
Circular Dichroism (CD)
Linear Dichroism (LD)
Magnetic Optical Rotatory Dispersion (MORD)
Magnetic Circular Dichroism (MCD)
Magnetic Linear Dichroism (MLD)
Fluorescence-Detected Circular Dichroism (FDCD)
Fluorescence-Detected Magnetic Circular Dichroism
Circular Polarization of Luminescence (CPL)
Fluorescence Polarization
Vibrational Circular Dichroism (VCD)
Raman Optical Activity (ROA or CID)
Ellipsometry
Photoelasticity
Polarimetry
Circular Differential Scattering
Linear Differential Scattering
Differential Polarization Microscopy
Doppler-Free Laser Polarization Spectroscopy

to describe light by the electric field alone. It also happens that the electric field interacts more strongly with matter, so this convention is well suited for discussions of spectroscopy.

For any transverse wave, the vibration remains perpendicular to the direction of travel. If the electric vector oscillates in a single plane, then the light is said to be plane polarized or linearly polarized. Figure 1a shows plane polarized light traveling along the z direction. If an observer looks toward the source, he sees that the electric vector traces out a line in the plane perpendicular to the propagation direction. Any polarization state can be resolved into two orthogonal linear polarizations. In Figure 1b, two linear components (one horizontal and one vertical) have a particular phase relationship such that the resultant beam is linearly polarized at 45° to the vertical.

The electric vector may follow other patterns. If the tip of the electric vector traces out a helix as it propagates, then circular polarization is implied. Figure 1c shows right circularly polarized light (RCPL). Here, the electric field traces out a right handed or clockwise circle as it propagates. As indicated in Figure 1c, the circularly polarized light can be resolved into horizontal and vertical linearly polarized components that have a phase difference of 90°. Left circularly polarized light (LCPL) would look similar to the RCPL except that the horizontal component would lag the vertical component by 90°, as opposed to leading by 90°, and the resultant vector would trace out a counterclockwise circle. In cases a-c the amplitudes of horizontal and

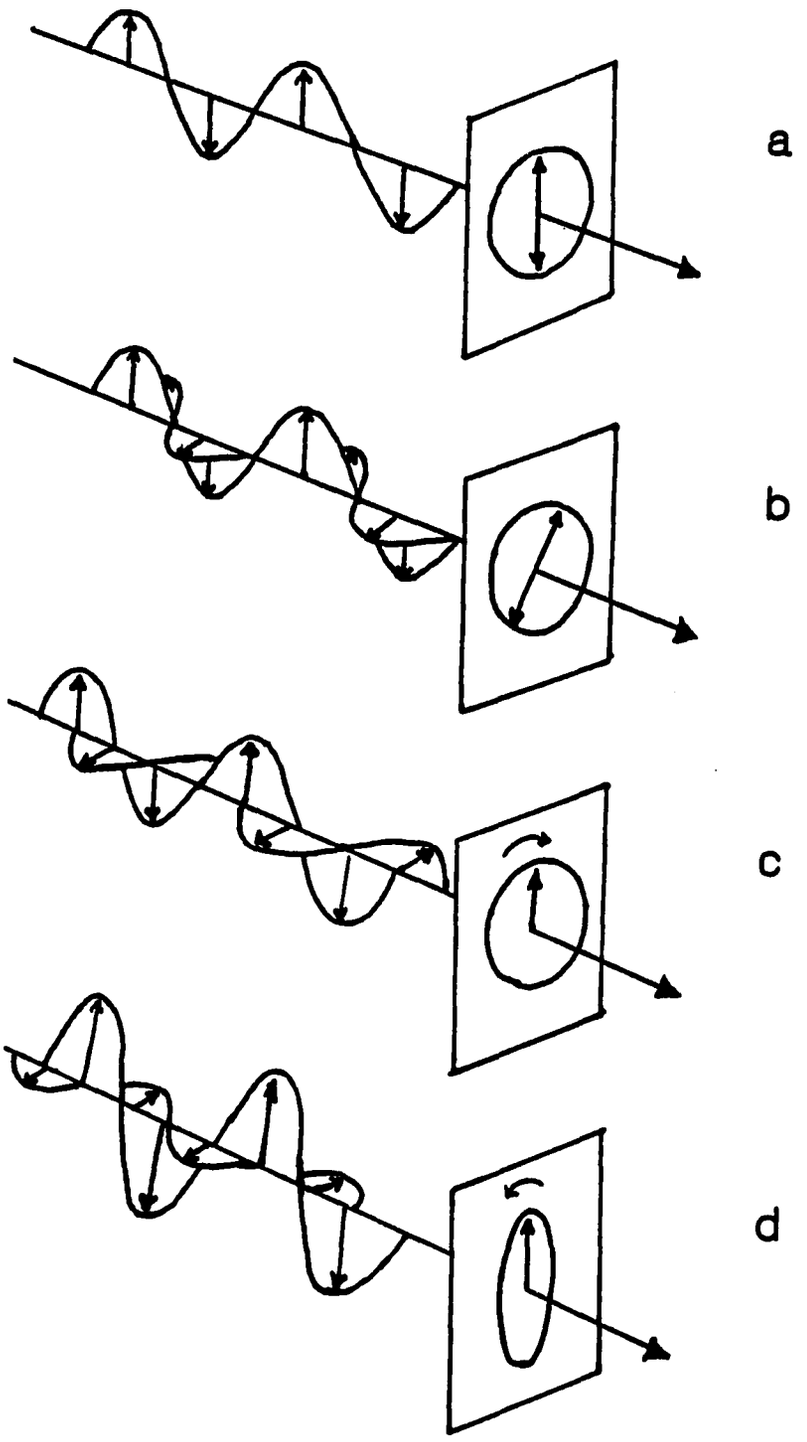

Figure 1. Polarization states: (a) linearly polarized at 0°, (b) linearly polarized at 45°, (c) right circularly polarized, (d) left elliptically polarized

vertical components are equal. If the components have different amplitudes, then the electric vector traces out an ellipse as shown in Figure 1d. In this example, the relative phase difference between linear components is the same as it would be for LCPL so that a left-handed ellipse is produced. The major axis of an ellipse will vary depending on the relative phase of the two components.

Elliptical polarization is the most general classification of polarization state. Linear and circular polarization states are actually special cases of elliptical polarization which exhibit particular amplitude and phase relationships. This treatment demonstrates the resolution of any polarization into a combination of orthogonal linear components. Alternatively, one could also think of resolving any polarization into a combination of circularly polarized forms with the appropriate amplitude and phase. The polarization states described here require a constant (fixed) phase relationship between components. A more thorough mathematical description of polarization is given in ref *1*.

Polarization, Retardance, and Modulation

An individual photon is polarized. The intrinsic spin (angular momentum) defines a photon's handedness, which is designated as right or left. Most light sources produce unpolarized light (or natural light) which actually contains polarized components varying rapidly and randomly in phase. In a tungsten light bulb, for example, the filament heats up and gives off photons in all directions with no specific phase relationship. Natural light can be modified to exhibit a degree of

polarization, however. Several types of polarizing devices are capable of producing partially polarized light from natural (unpolarized) light.

Polarization can be achieved by four different mechanisms: reflection, dichroism, scattering, and birefringence. If we consider any light to consist of two orthogonal components, then discrimination of one component by some asymmetric process will result in polarized light. Reflection and scattering work in this way to partially polarize natural light. The pile of plates polarizer relies on multiple reflections at a specific angle of incidence to produce polarized light. Dichroism, the preferential absorption of one polarization over another, is utilized in a variety of plastic sheet polarizers (polaroid films). Wire grid polarizers, which are useful for polarization of infrared radiation, are also based on dichroism. A large class of polarizers are made of crystalline materials which are birefringent. Birefringent materials are optically anisotropic because they exhibit two different indices of refraction along different crystal axes. This property can be used to physically separate two orthogonal components of a polarized light beam. Calcite polarizing prisms are classic examples of birefringent polarizers.

Linear polarizers are the most common type of polarizer, but circular and elliptical polarizers exist as well. The latter forms require the use of polarization retarders (see below). The plastic film in glasses used for viewing 3-D films is actually a circular polarizer. Many options are available when choosing a polarizing device; however, the attainable polarization purity varies greatly for different types of

polarizers. Calcite prism polarizers provide high degree of polarization and are typically rated to pass less than 1 part in 10^6 of the undesired polarization. Some dichroic film polarizers provide only about 1 part in 100 rejection. Wavelength and power must also be considered when choosing a polarizer to assure compatibility (*2*).

Once light has a defined polarization, it can be converted into other polarization states with the use of an optical phase retarder such as a wave plate or a Fresnel rhomb. Retardation devices introduce a phase delay between orthogonal components of the incident light. This can be visualized by referring back to Figure 1. A 90° shift in phase of the horizontal component relative to the vertical component converts linear polarization (Figure 1b) to circular polarization (Figure 1c) This 90° (¼-wave) shift is the result produced by action of a quarter-wave plate. In wave plates, the phase shift is due to birefringence. Hence, the amount of retardation depends on the optical path length and is wavelength specific. The Fresnel rhomb produces a 90° phase shift based on total internal reflection. In this case, retardance is uniform over a wider wavelength range.

Modulation of polarization refers to alternating between two well-defined polarization states at a chosen frequency (rate). The principles of polarization and phase retardance are applicable in the development of polarization modulators. A variety of modulation devices are available. Some of the common techniques for modulating polarization are the Faraday effect, Kerr effect, Pockels effect, and photoelasticity. The Faraday (also called magneto-optic) effect

involves the rotation of linear polarization in a magnetic field. This is the principle used in the laser based polarimeter (*3*). An alternating current in a coil induces an alternating magnetic field, which in turn causes the polarization plane to alternate.

The Kerr and Pockels effects are based on electrooptic phenomena and are described in greater detail in refs *1* and *4*. The Kerr effect involves isotropic crystals (and some liquids), which become birefringent when placed in an electric field. If the electric field is modulated, then the polarization of a light source passing through the medium will be modulated. Placement of a fixed linear polarizer after the modulator converts the polarization modulation to amplitude modulation. In this way, Kerr cells operate as fast optical shutters and are used in many pulsed laser systems. The amount of birefringence produced in the Kerr effect is proportional to the square of the electric field. Hence, it is also referred to as the quadratic electrooptic effect.

The Pockels effect occurs only in certain asymmetric crystals. Here, birefringence is directly proportional to the applied field. The Pockels effect is commonly named the linear electrooptic effect. In both of these modulators, the applied voltage is varied to regulate retardance and polarization modulation for a given wavelength. The electrooptic modulators can be operated in a wide frequency range (up to 10^{10} Hz) which makes them very versatile.

Lastly, the photoelastic modulators (PEMs) are derived from transparent isotropic materials which become birefringent under

mechanical stress. Photoelastic modulators must be operated at a specified oscillation frequency which is characteristic of the optical material (*5*). This renders them somewhat less versatile than the electrooptic modulators, but they have the advantages of wider acceptance angle and lower power requirements.

Although natural light from many sources can be polarized, laser sources provide some unique advantages for polarization modulation. The lasing action forms a coherent chain of highly monochromatic photons. Lasers are commonly designed with Brewster angle windows which allow only plane polarized light to be reflected and thereby amplified (*6*). This results in very high linear polarization purity. Hence, alteration of polarization state by a retarder or modulator can be very efficient. Because retardance is often a function of wavelength, the monochromaticity of laser sources further improves the efficiency of polarization modulation.

The topics covered in this dissertation make use of the selective interactions of alternating polarizations. Chapter II deals with laser Doppler-free polarization spectroscopy, in which absorption of a circularly polarized pump field induces an optical anisotropy in an atomic sample. A second linearly polarized probe beam undergoes a measurable change in polarization as it interacts with the anisotropic environment. Chapters III and IV center on the development of fluorescence-detected circular dichroism (FDCD) for use as an on-column detector in capillary electrophoresis. FDCD selectively probes chirality in fluorescent molecules. The themes common to the two

techniques are laser polarization modulation and lock-in detection for improved selectivity and detectability.

CHAPTER II. IMPROVEMENTS IN POLARIZATION SPECTROSCOPY BASED ON HIGH-FREQUENCY MODULATION

Introduction

Trace analysis is of great interest in a variety of fields ranging from environmental and clinical analysis to industrial process monitoring. The quest for lower detection limits has been pursued by modifications of traditional techniques and the development of new techniques. As analysts develop more sensitive methods, the specificity requirements increase as well. A background or noise component in an absorbance measurement may have negligible effects on the signal generated by an analyte at ppm concentrations, but it may severely hinder the determination at analyte concentrations 1000 times lower. In spectroscopic methods, lasers have the advantage of being highly monochromatic. This makes them capable of exciting very specific transitions in a species of interest. Hence, they allow the spectroscopist to develop methods with high specificity and may reduce the amount of sample preparation required to eliminate the adverse effects of impurities.

One technique that exhibits both high sensitivity and specificity is Doppler-free laser polarization spectroscopy, first demonstrated by Wieman and Hänsch (*7*). Closely related to saturated absorption spectroscopy (*8-10*), this method uses two counterpropagating laser beams which overlap in the sample region as depicted in Figure 2. In the simplest case, both beams are tuned to an absorption transition of the atoms (or molecules). The higher power pump beam is circularly

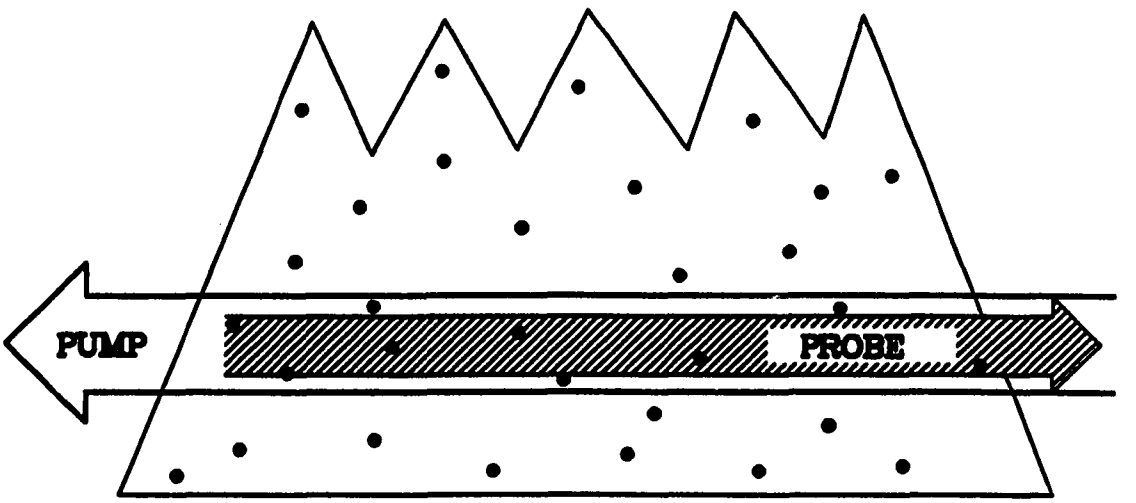

Figure 2. Counterpropagating pump and probe beam arrangement for Doppler-free laser polarization spectroscopy in an analytical flame
Signal is derived only from those analyte species interacting with both beams simultaneously.

polarized, but could also be linearly polarized at 45° to the probe beam polarization. It induces an optical anisotropy in the sample by depleting the analyte populations in certain sublevels. The left and right circular components of the linearly polarized probe beam sense this anisotropy as differences in absorption coefficients and refractive indices. This results in a change in the polarization plane of the probe beam, which can be measured as increased transmission through a crossed polarizer, frequently called an analyzer. The amount of probe light reaching the detector is related to the number of analyte species present. The technique is Doppler-free because only those analyte species having zero velocity along the direction of propagation will interact with both light beams simultaneously giving rise to signal. In practice, some Doppler broadening is observed due to the finite crossing angle of the pump and probe beams.

Our group previously applied this technique to elemental analysis in a flame using a continuous wave (cw) ring dye laser (*11*). The polarization of the pump beam was modulated between left and right circular polarizations at a frequency of 800 Hz and detection was via a lock-in amplifier. The reported limits of detection (*S/N* = 2) of 30 ng/L and 37 μg/L for sodium (D_1) and barium respectively are comparable to limits of detection obtained by atomic fluorescence techniques. More recently, Lanauze and Winefordner (*12*) applied a wider bandwidth pulsed (excimer pumped) dye laser with boxcar averaging detection to the determination of sodium (D_2) by polarization spectroscopy. They obtained a 2 μg/L detection limit (*S/N* = 3) by averaging 3000 pulses.

Lanauze and Winefordner reported that a poor extinction ratio (1:200) severely limited their system. In comparison, the polarimeter system developed by our group has been shown (*3*) to have extinction ratios as high as $1:10^{10}$. This improved extinction ratio certainly figures significantly in the improvement seen in the cw (*11*) vs. the pulsed (*12*) laser systems. Typically, extinction ratios deteriorate substantially as the number of optical components between the polarizers increases. Because of this, we choose configurations which minimize the number of surfaces and thereby limit additional birefringence between the two polarizers. In the pulsed laser system (*12*), several optical components are placed between the polarizers, and it is likely that this contributes to the poor extinction ratio observed.

The limiting noise in the pulsed laser experiment is the pulse-to-pulse variation in power that is commonly seen in such lasers. The limiting noise in the cw laser system can be attributed to flicker in the probe beam. High frequency modulation (>100 kHz) with cw lasers has been shown to improve detectabilities in polarimeters (*13*) and other laser based detectors (*14-16*) by reducing the effect of flicker noise. It is therefore reasonable to assume that similar improvements could be seen for polarization spectroscopy at higher modulation frequencies. In this paper, results are presented showing an improvement in the limit of detection for polarization spectroscopy based on this principle.

Theory

Doppler-free laser polarization spectroscopy was first demonstrated as a high-resolution spectroscopic technique (*7*). Early applications

centered around precise measurements of spectroscopic fine structure (*7*, *17-19*) and evaluation of physical constants (*20*). In light of this, it is not surprising that most of the early theoretical descriptions did not emphasize the nature of the relationship between the measured signal and the concentration of the absorbing species. In the present study we investigate this relationship to substantiate the usefulness of polarization spectroscopy for trace elemental analysis.

The atomic level diagram in Figure 3 is useful for describing the features of polarization spectroscopy. In this simple case, atoms undergo electric dipole transitions between the angular momentum quantum levels $J = 1$ and $J = 0$, where the lower ($J = 1$) level is made up of three degenerate orientational sublevels. These sublevels are designated by orientational quantum number m having the values -1, 0, and +1. The upper state ($J = 0$) has a single orientational level with $m = 0$. When an electronic transition occurs upon absorption of light, the change in angular momentum of the electron is dependent on the angular momentum of the absorbed photon. The intrinsic angular momentum of a photon is due to its spin and gives rise to the handedness we observe as left and right circularly polarized light.

If the direction of light propagation is chosen as the quantization axis, then right and left circularly polarized photons will have opposite spin projections. Using historical convention (*21*), the transition from $m = -1$ to $m = 0$ ($\Delta m = +1$) arises from absorption of a left circular photon, while the $m = +1$ to $m = 0$ ($\Delta m = -1$) transition results from absorption of a right circular photon. The $m = 0$ level of

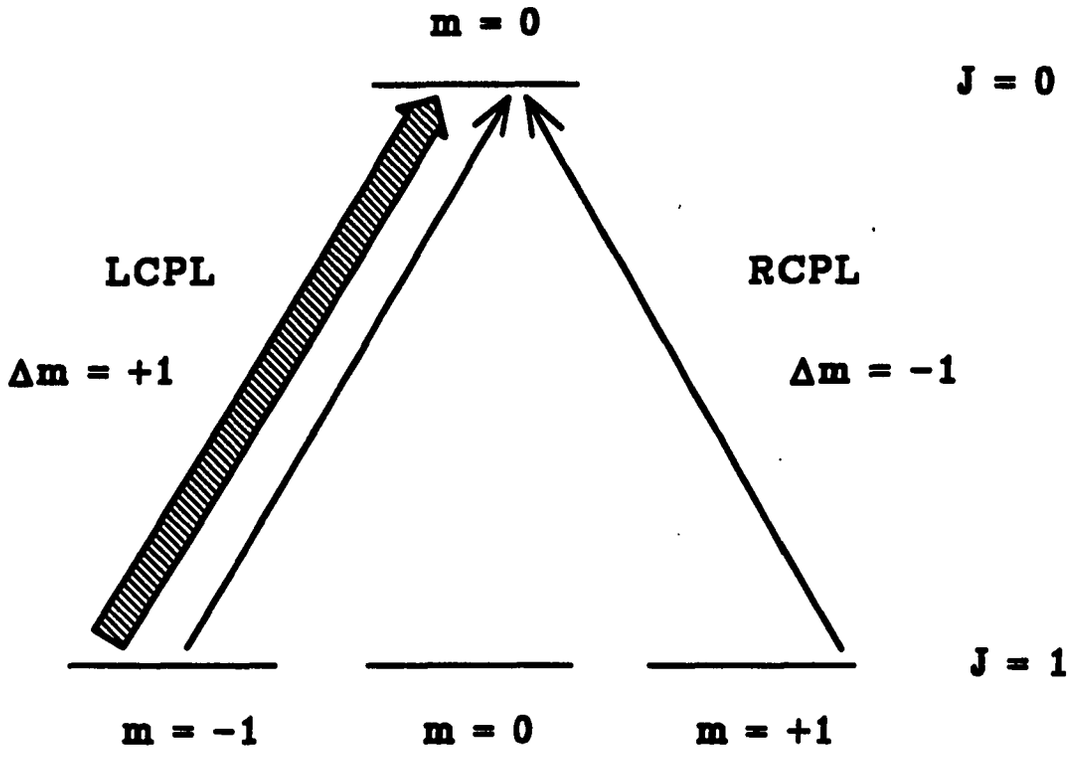

Figure 3. Atomic level diagram for atoms undergoing transitions from a $J = 1$ level to a $J = 0$ level
The presence of a left circularly polarized saturating beam depletes the population of the $m = -1$ state relative to the $m = +1$ state causing changes in absorption coefficients ($\Delta\alpha^+$, $\Delta\alpha^-$) and refractive indices (Δn^+, Δn^-).
LCPL and RCPL indicate left circularly polarized light and right circularly polarized light, respectively.

the lower state cannot couple to the radiation field under the quantization parameters set forth here (*22*). However, the $m = 0$ to $m = 0$ transition can occur in a linearly polarized field propagating in a direction different from the quantization axis. Other transition schemes, both atomic and molecular, which impart some degree of polarization selectivity are possible and can also be studied by Doppler-free laser polarization spectroscopy.

If we introduce a left circularly polarized pump beam, it saturates the $\Delta m = +1$ transition. Then, the left and right circular components of a linearly polarized probe beam sense the pump-induced anisotropy. Two different phenomena may be observed in these polarization spectroscopy experiments. The first is a dichroism effect. The left circularly polarized pump beam selectively saturates one transition relative to the other, causing the left circular component of the probe beam to see a reduced absorption cross-section. This produces slight changes in the absorption coefficients for the left ($\Delta\alpha^+$) and right ($\Delta\alpha^-$) circular components of the probe beam as it passes through the anisotropic sample. Reduced absorption of one component relative to the other results in a slight increase in overall intensity of the probe beam and produces elliptical character in the probe polarization. Some of this light is transmitted by the analyzer, producing a signal at the detector. This dichroism signal has a Lorentzian line shape (determined by lifetime broadening or pressure broadening) which can be observed by varying the dye laser frequency and recording the absorption spectrum.

The second effect is due to dispersion, or birefringence, a difference in refractive indices for the two circular components of the probe beam. The changes in refractive index (Δn^+, Δn^-) result from an anisotropic distribution of angular momentum orientations. Absorption of the circularly polarized pump induces nonuniformity in populations of the orientational (m) sublevels. The birefringence causes a rotation of the polarization plane of the probe beam and thereby increases the amount of light passing through the analyzer. This birefringence effect produces a dispersion-shaped signal as a function of frequency.

A mathematical description is helpful in understanding these signals. Making the assumptions that the probe beam is weak and does not change the optical properties of the sample and that the pump-induced anisotropies are small, one can express the probe beam intensity (I_T) transmitted by the analyzer as (*7*)

$$I_T = I_0 \left[\theta^2 + \theta \frac{s}{2} \frac{\chi}{(1 + \chi^2)} + \left[\frac{s}{4} \right]^2 \frac{1}{(1 + \chi^2)} \right] \qquad (1)$$

Here, I_0 is the probe intensity and θ is the angle of offset of the analyzer transmission axis from the exactly crossed position, also called the uncrossing angle. The detuning of the laser frequency from resonance is given by χ, defined as

$$\chi = (\omega - \omega_0)/\gamma \qquad (2)$$

where ω_0 is the resonant frequency and γ is the natural or the pressure-broadened line width, whichever is the larger. The quantity s, which

contains information related to sample concentration, path length and pump power, is given by

$$s = -\tfrac{1}{4}(1 - d)\alpha_0 l I/I_{sat} \tag{3}$$

The unsaturated background absorption of the probe, α_0, is directly proportional to N^0, the total number density of absorbers in the ground state, and is therefore proportional to concentration, C. The absorption path length is l, and the pump beam intensity is I. The term I_{sat} refers to the saturation intensity, which gives a measure of the ease with which the pumped transition may be saturated. The parameter d is defined by

$$d = \frac{\Delta\alpha^-}{\Delta\alpha^+} \tag{4}$$

and is a measure of the magnitude of the anisotropy, which depends on the angular momenta and decay rates of the states involved.

Substituting equations 3 and 4 into equation 1 gives

$$I_T = I_0 \left\{ \theta^2 + \frac{\theta}{2}\left[-\frac{1}{2}\left[1 - \frac{\Delta\alpha^-}{\Delta\alpha^+}\right]\alpha_0 l I/I_{sat}\right]\frac{\chi}{(1+\chi^2)} + \left[\frac{1}{4}\right]^2\left[-\frac{1}{2}\left[1 - \frac{\Delta\alpha^-}{\Delta\alpha^+}\right]\alpha_0 l I/I_{sat}\right]^2 \frac{1}{1+\chi^2}\right\} \tag{5}$$

Here, the concentrations are low and the dichroic attenuation term for I_0 can be neglected. The first term will be a constant for a given analyzer rotation. The second term describes the dispersion-shaped

signal. The refractive index change, $\Delta n^{\pm} = \Delta n^{+} - \Delta n^{-}$, can be related to the dichroism, $\Delta\alpha^{\pm} = \Delta\alpha^{+} - \Delta\alpha^{-}$, by the Kramers-Kronig (*7,11*) relation such that

$$\Delta n^{\pm} = -\tfrac{1}{2}\Delta\alpha^{\pm}\chi c/\omega \qquad (6)$$

The last term in equation 5 describes the Lorentzian-shaped dichroism signal. When the polarizers are perfectly crossed, $\theta = 0$, and the third term leads to a purely Lorentzian signal. If the analyzer is offset from extinction so that θ dominates over s, the last term becomes insignificant and a dispersion-shaped signal is observed. Thus, selection of the analyzer transmission axis allows observation of a signal that is due to the effect of dichroism or birefringence alone. At intermediate θ values, the signals will reflect a combined effect.

From equation 5 it is evident that the dichroism signal depends on the square of the concentration of the absorbing species, as the s term is squared. In contrast, the dispersion signal is linearly dependent on C. These relationships have been experimentally verified for sodium concentrations in the range 100-1000 ppm (*12, 23*). It is also interesting to note the signal dependence on laser power. Equation 5 shows that the signal intensity for the Lorentzian term is proportional to $I_0 I^2$ and therefore should increase as the cube of the laser power. The dispersion term increases as $I_0 I$ and shows a square dependence on the laser power.

In practice, the finite extinction ratio ξ also contributes to the total intensity at the detector. The term $I_0\xi$ should be added to the

right hand side of equations 1 and 5 to correct for this. However, because the extinction ratio remains constant for a given optical alignment and only differences in the intensity are measured, this $I_0\xi$ term does not invalidate the linear relationships for signal vs. C^2 in the Lorentzian mode and signal vs. C in the dispersion mode, as described above. It does, however, affect the signal vs. power, P, relationships, and the measured signals do not exhibit exact P^3 and P^2 dependence for the Lorentzian and dispersion modes, respectively, unless $I_0\theta^2$ and $I_0\xi$ are first subtracted from the total signal. Several papers dealing with polarization spectroscopy (*10*, *17*, *24*) present equation 5 with two additional terms containing I_0b^2 and $I_0b\Delta\alpha_0 l$, where b accounts for any extra birefringence introduced by sample windows or other optical components between the polarizers. Since such components are absent in our system, $b = 0$, and we omit the b terms from equation 5.

It is clear that one can obtain larger signals by working well away from the extinction position. In fact, θ should be as large as possible. The noise, however, increases as θ increases, because of the residual intensity transmitted to the phototube. A good compromise is to increase θ to the point where flicker noise in the transmitted probe beam becomes comparable to, but not larger than, the noise from other sources. Since flicker noise here is drastically reduced by high-frequency modulation, a gain in detectability over earlier work (*11*) is obtained by working off-null.

Experimental

Optical system

A schematic diagram of the experimental system is shown in Figure 4. It is very similar to the previous system (*11*). An argon ion laser (Control Laser, Orlando, FL, Model 554A) serves as the pump laser for the ring dye laser (Spectra Physics, Mountain View, CA, Model 380A). The ring laser is operated with Rhodamine 6G dye (Eastman Kodak Co., Rochester, NY) and tuned to the sodium D_1 resonance line.

The dye laser beam is divided into three portions by a beam splitter. The first weak reflection from the beam splitter is used as the probe beam. The noise is proportional to the probe beam intensity, so, it is better to have more light in the pump beam for a given total laser output. The probe beam passes through a 50-cm focal length lens and then through selected positions on the Glan-Thompson polarizer and analyzer prisms (Karl Lambrecht Corp., Chicago, IL, Model MGT-25-E8-90). The focal point of the probe beam lies half way between the crossed polarizers at the center of the 6-cm slot burner (Varian Techtron, Palo Alto, CA, Model 02-100035-00). The polarizers are mounted in rotational stages (Aerotech Inc., Pittsburgh, PA, Model ATS-301R) having 0.0006° resolution. The rotational stages and burner are mounted on 5/8 in. thick aluminum plates extending from the edge of the optical table (Newport Research Corporation, Fountain Valley, CA) so that the flame can be positioned low enough to allow a more rigid mounting of the optical components. The portion of the probe beam that passes through the analyzer prism is directed through a pinhole aperture, a cylindrical

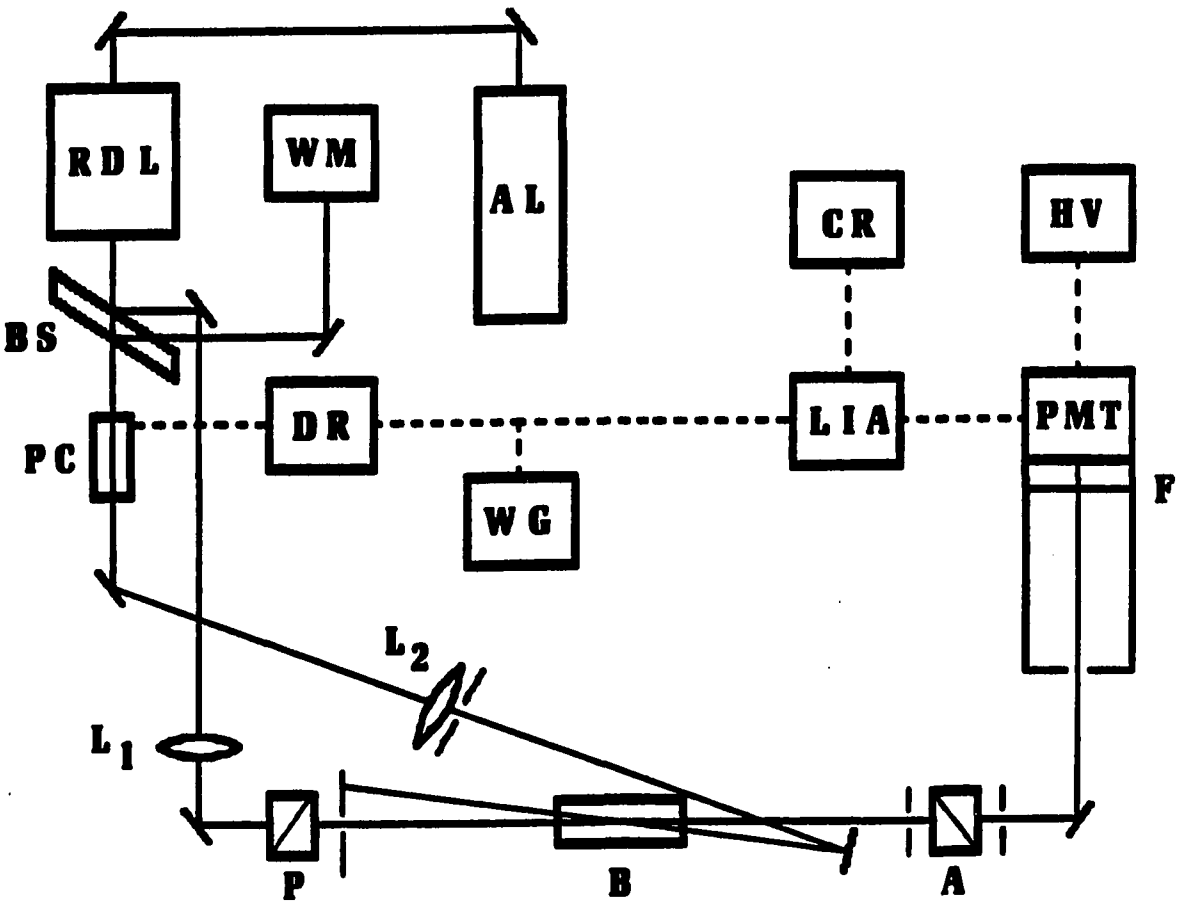

Figure 4. Experimental system for atomic polarization spectroscopy Solid lines indicate optical paths and broken lines show electrical connections. (A) Analyzer Prism, (AL) Argon Laser, (B) Slot Burner, (BS) Beam Splitter, (CR) Chart Recorder, (DR) High-voltage Driver, (F) Line Filter, (HV) Power Supply, (L_1 and L_2) Focusing Lenses, (LIA) Lock-in Amplifier, (P) Polarizer Prism, (PMT) Photomultiplier Tube, (RDL) Ring Dye Laser, (WG) Waveform Generator, (WM) Wavemeter.

light tunnel and a line filter (Promfret Research Optics, Inc., Orange, VA, Model 11-5890-1) before reaching the photomultiplier tube (PMT) (Hamamatsu, Middlesex, NJ, Model R928). The PMT is operated at -1000 V dc by a high voltage power supply (EMI Gencom Inc., Plainview, NY, Model 3000R). The second weak reflection from the beam splitter is directed to a wavemeter (Burleigh Instruments, Fishers, NY, Model WA-20) for wavelength calibration.

The major portion (80%) of the dye laser beam, the pump beam, passes through the beam splitter and the Pockels cell electrooptic modulator (Lasermetrics Inc., Teaneck, NJ, Model 3030). This pump beam is also focused by a 50-cm focal length lens and overlaps the probe beam as it counterpropagates through the flame. The pump beam strikes a black beam stop on the back side of the polarizer mount after passing through the flame. Several other pinhole apertures are placed along the beam paths to minimize the stray and scattered light reaching the detector. A black shield completely encloses the region from the analyzer stage to the back side of the PMT enclosure to reduce background from the dye laser cavity. To further reduce scatter from the pump beam, the sides and back of the last reflecting mirror are painted black. The crossing angle between pump and probe beams is minimized to optimize the degree of overlap within the flame.

The linear polarization of the pump beam is modified to create left and right circularly polarized light (LCPL and RCPL) by the action of the Pockels cell. By proper alignment of the Pockels cell and appropriate selection of driving voltages, one can produce LCPL and

RCPL without the need for a Fresnel rhomb (*25*). The required voltages are provided by a high voltage driver (Conoptics, Danbury, CT, Model 25) driven by a +1-volt pulse at 150 kHz from a waveform generator (Wavetek, San Diego, CA, Model 162). This makes the present system simpler than that described previously and allows more stable modulation at high frequencies (*11*). To verify the modulation of LCPL and RCPL, a Fresnel rhomb (Karl Lambrecht Corp., Chicago, IL, Model ER4-25-580) and a Promaster polarizing filter (Photographic Research Org. Inc., Fairfield, CT) are placed in the pump beam near the burner. The rhomb converts LCPL and RCPL into horizontal and vertical linearly polarized light. The polarizer discriminates between the linear polarizations, producing amplitude modulation. After passing through a neutral density filter of optical density 0.5, the degree of modulation is detected by a photodiode (Hamamatsu Corp., Middlesex, NJ, Model S1790) and displayed on an oscilloscope (Tektronix, Beaverton, OR, Model 7904). The signal from the PMT is sent to a lock-in amplifier (EG&G PARC, Princeton, NJ, Model 5202) which is also synchronized to the modulation frequency of the waveform generator. A 1- or 10-second time constant is used. The demodulated signal from the lock-in amplifier is displayed on a chart recorder (Measurement Technology Inc., Denver, CO, Model CR452).

Reagents

A standard stock solution of sodium (2.403 g/L), prepared by dissolving electrolytic sodium hydroxide pellets (Fisher Scientific Co., Fairlawn, NJ) in quadruply distilled demineralized water and stored in a sealed polyethylene bottle, was used. Standard sodium solutions were

prepared by diluting this stock solution with distilled demineralized water that had been purified by a four-cartridge Milli Q system (Millipore Corp., Bedford, MA). The demineralized water contains trace amounts of sodium, so the standards are actually sodium addition standards. Calibration standards were prepared in the range 9.612-96.12 ng/mL added sodium, stored in polyethylene bottles and used the same day as prepared.

The standard solutions were aspirated into a laminar air-acetylene flame at a rate of 8.4 mL/min for optimum signal amplitude. The optimized air:acetylene ratio was 4.8:1.0 as measured on gas flowmeters (Emerson Electric Co., Hatfield, PA, Model 1355-00A1FAA).

Data collection procedure

The various components in this experimental system are optimized separately before any polarization spectra can be obtained. Alignment of the argon laser and dye laser is set to achieve maximum output power at the desired wavelength. The argon laser is servo controlled at 4.0 W to increase power stability. This produces about 80 mW total dye laser power at 589.757 nm, the vacuum wavelength for the sodium D_1 line as measured by the wavemeter. The probe beam is carefully directed through positions on the polarizer and analyzer previously found to give the optimum extinction ratio. With the polarizer axis set to give the highest transmission of the horizontally polarized probe beam, total probe laser power in the cavity between the polarizers is 7.5 mW. Fine tuning of the analyzer is accomplished by monitoring the PMT current (extinction current) while rotating the analyzer transmission axis. The

crossed position is determined as that giving the lowest extinction current reading, typically about 1.0 μA. This (maximum extinction) alignment is used when obtaining Lorentzian-shaped dichroism signals. For observing the dispersion-shaped birefringence signals, the analyzer is rotated 0.040° counterclockwise away from extinction. Under this condition, the PMT current is about 64 μA. The pump beam is directed to overlap with the probe in the flame, and the modulation is optimized by adjusting the Pockels cell position and the driver input and bias voltages to produce approximately 95% modulation between left and right circularly polarized light.

To set the detection electronics, a solution containing sodium is aspirated into the air-acetylene flame. The PMT signal is connected to the lock-in amplifier and the phase settings are optimized while the dye laser is tuned to the absorption maximum. Final adjustments of burner position, pump beam overlap with probe, and the Pockels cell bias voltage are necessary to produce the maximum sodium signal. Proper shielding from scattered pump and flame emission is critical in obtaining good signal-to-noise (*S/N*) ratios. Baseline noise is observed on a more sensitive scale to verify that light scattering from the pump laser is not the limiting noise source. When these preliminary optimizations are complete, the dye laser wavelength is set to the starting frequency of the 30-GHz scan range. Sodium spectra are collected as the wavelength is scanned from 589.772 to 589.738 nm (vacuum λ). Scan times vary from 40 to 400 seconds.

Results and Discussion

The primary goal in this work was to improve the limit of detection found in the earlier work (*11*) by using higher modulation frequency and a more stable optical system. The modulation electronics used in the work described here are suitable for high frequencies, whereas those used earlier were limited to operation at or below 800 Hz. The Conoptics driver is capable of very stable Pockels cell voltage modulation into the MHz range. The actual voltages applied to the Pockels cell are in the range from -200 to +200 V. A high-frequency lock-in amplifier enables the use of frequencies above 100 kHz. In the present work, the Pockels cell produces highly efficient (>90%) modulation between LCPL and RCPL without the need for the Fresnel rhomb which was used earlier. The reduction in the number of optical components needed makes the alignment procedure simpler and may improve alignment stability as well. In addition, without the rhomb, the pump and probe overlap angle can be made smaller, which should produce narrower line widths and a longer interaction length. The former can be important in experiments where high spectral resolution is critical, but line width comparisons were not made in this study.

Stability of optical alignment is of concern here because the extinction ratio of the polarizers is highly dependent on beam position. In other polarimeter systems, excessive baseline noise has been caused by unstable optical mounts. Therefore, in contrast to the arrangement used earlier (*11*), all optical components are mounted close to the table top on short rigid mounts.

Since sodium-free water was not available, distilled, demineralized Millipore-filtered water was used in these studies. The amount of sodium in an early sample of this water was found to be 27 μg/L by ICP-MS analysis using a standard addition method. Initially, a crossed-polarizer arrangement was employed to examine Lorentzian-shaped dichroism signals for the sodium D_1 line. An example of a Lorentzian signal for sodium is shown in Figure 5a. Lorentzian signals were obtained at three different laser power levels (from 30 to 80 mW) for a series of four standards containing 0-100 μg/L added sodium. Each data set indicated that the Lorentzian signal, S_L, has a strong dependence on C^2. Linear regression analysis gave $r \geq 0.999$ for S vs. C^2 in each of these runs. This confirms the findings reported by another group for a pulsed laser system (*12, 23*). It also shows agreement with equation 5 and is the expected behavior.

To evaluate the dependence of the dispersion signal, S_D, on concentration, the analyzer was rotated counterclockwise from the extinction position to $\theta = 0.040°$. Figure 5b shows a dispersion signal for sodium in distilled demineralized water. Clockwise rotation of the analyzer produced dispersion signals of the same magnitude and opposite symmetry. Although larger dispersion signals can be obtained with larger analyzer offset angles, the baseline noise also increases. We found 0.040° to be a suitable angle for collecting dispersion spectra while maintaining a good *S/N* ratio. Each dispersion signal, S_D, was measured as the peak-to-trough magnitude for the scan. As expected, a linear relationship was observed between S_D and C.

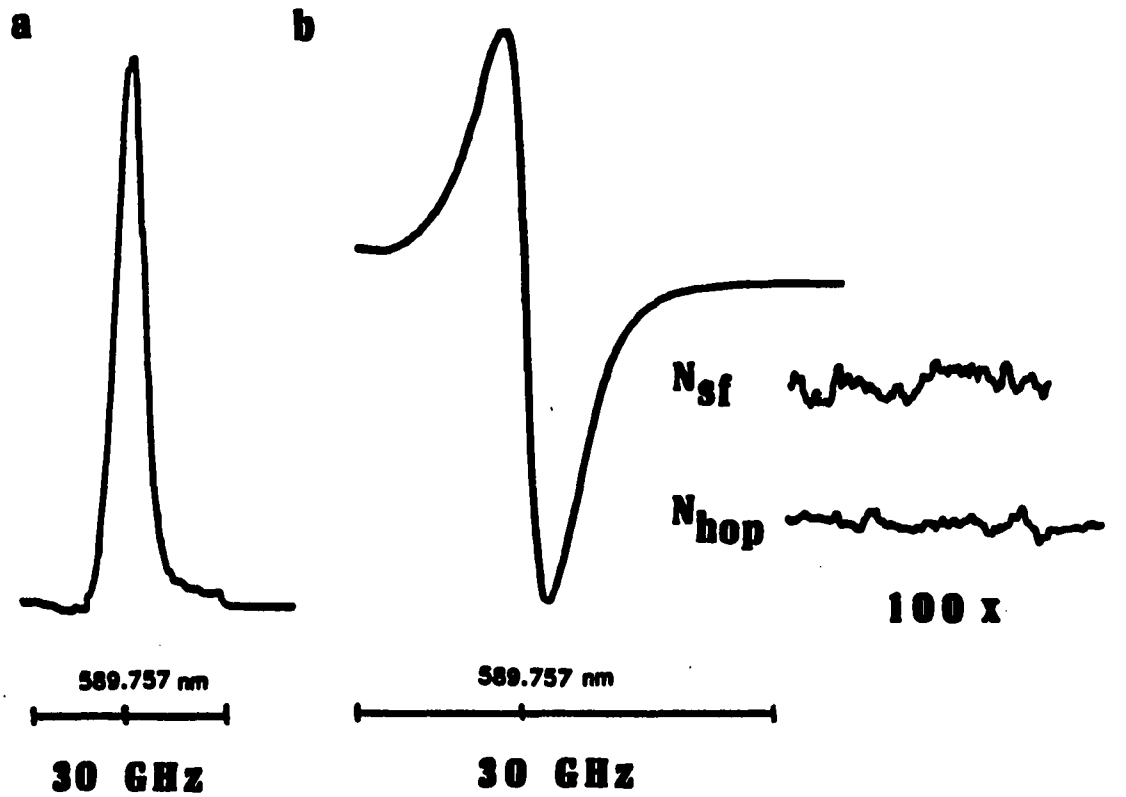

Figure 5. Polarization signals for Na at 1.95 μg/L
(a) Lorentzian signal for $\theta = 0°$.
(b) dispersion signal for $\theta = 0.040°$.
Noise in (b) is expanded 100 times.
See text for details.

While examining these relationships and attempting to maximize the *S/N* ratios for optimum detectability, we observed that the baseline noise at the starting frequency of the laser scan, N_{sf}, increased as the sodium concentration increased from 10 to 100 μg/L. One possible explanation is that because sensitivity is very high, N_{sf} is actually caused by the fluctuating sodium signal in the wings of the absorption line. If this is the case, then one can expect even less noise at a wavelength further removed from the absorption maximum. To pursue this, the ring laser was tuned from 589.772 nm, which corresponds to the starting frequency, to 589.684 nm, which is one etalon mode separation ("hop") of 75 GHz away. The total laser power and the extinction current remained constant, so noise comparisons are valid. At the second wavelength, the baseline noise, N_{hop}, remained relatively constant for the same set of concentration standards. Because the absolute light levels at the detector are smaller in the Lorentzian mode, the increase in N_{sf} with concentration is less obvious than in the dispersion mode. Since a measure of true baseline noise fluctuations at the maximum absorption wavelength, λ_{max}, in the absence of signal is not possible (because some sodium is always present), N_{hop} is chosen as the relevant noise measurement for the S/N_{hop} and limit of detection (LOD) calculations. Although Lorentzian and dispersion S/N_{hop} ratios for the distilled water are similar, the dispersion signal facilitated straightforward standard addition analysis and extrapolation to the LOD because of the linear relationship between S_D and C. Furthermore, the dispersion signal is larger because of the square term in equation 5.

For these reasons, the dispersion mode was employed in the final optimizations and LOD determination.

A second sample of the distilled demineralized water was obtained. By comparison of dispersion signals, the new sample had a substantially lower sodium concentration than the first sample. Fresh sodium addition standards were prepared with the this new sample. All experimental parameters were optimized for maximum S_D/N_{hop} at 150 kHz modulation frequency and 80 mW total laser power. At this power, the pump and probe powers were 65 and 7.5 mW, respectively. Dispersion signals were obtained in triplicate for the water sample and for seven other addition standards with 10-100 μg/L added sodium. The precision of this analysis is characterized by an average RSD of 2%, and good qualitative reproducibility of spectral line shape is observed. The results of this analysis are displayed graphically in Figure 6. Linear regression analysis of this data set for S_D (μV) vs. C (μg/L added sodium) gives a straight line of slope 222 $\mu V \cdot L \cdot \mu g^{-1}$ and intercept 520 μV. The correlation coefficient, r, is 0.9955. The calculated amount of sodium present in the water is 1.95 μg/L, as determined from the x-axis intercept in this standard addition method. Also included in Figure 6 are the noise measurements made at the start frequency and the mode hop frequency for the different concentration standards (see discussion above).

Once the concentration of sodium in the distilled, demineralized water is known, the S_D/N_{hop} ratio of this sample is used to calculate the LOD for sodium at $S/N = 2$. The actual dispersion signal obtained

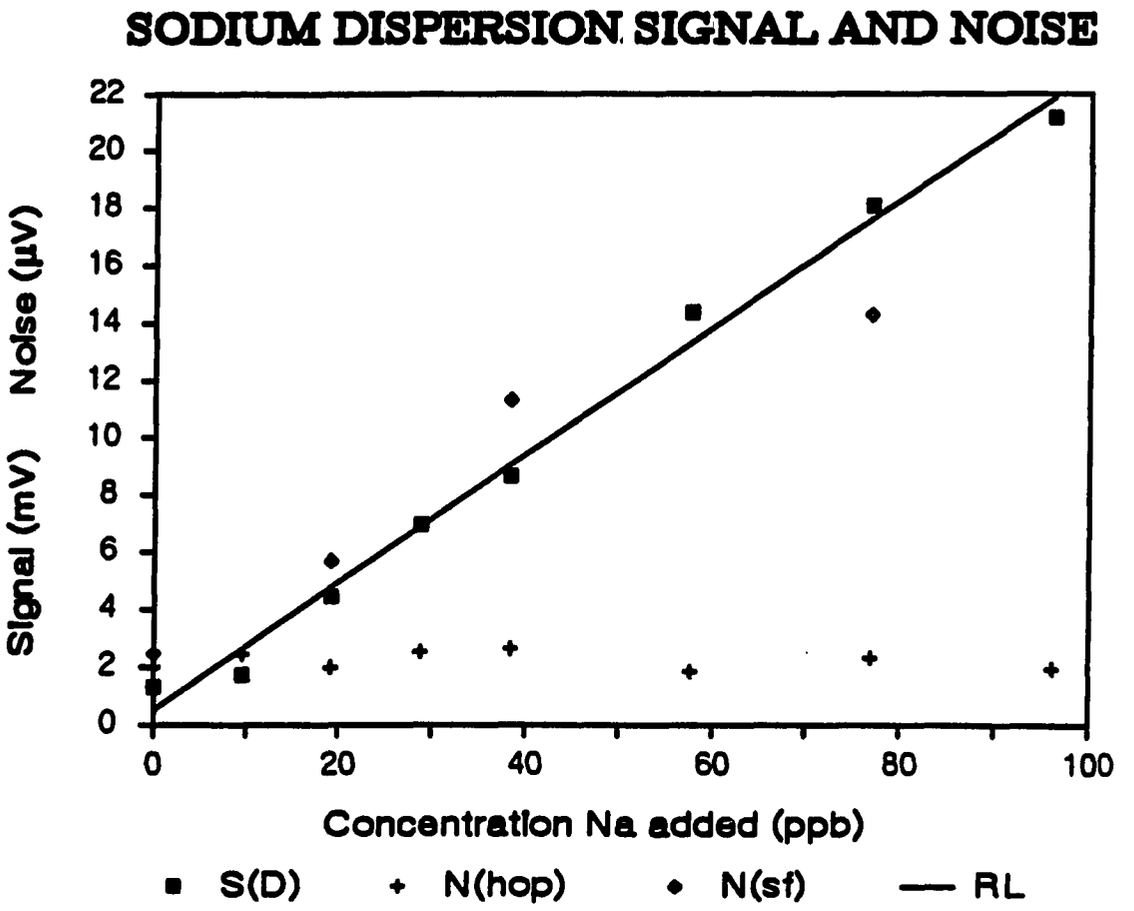

Figure 6. Plot of dispersion signal and noise vs. sodium concentration S(D) is the average peak-to-trough magnitude of the sodium dispersion signal obtained for three trials. N(hop) is the noise measured at the mode hop position (589.684 nm). N(sf) is the noise measured at the start frequency position (589.772 nm). RL is the calculated linear regression line.

for this sample under the conditions described above using a 10-second time constant is shown in Figure 5b. Both N_{sf} and N_{hop} are also shown at higher sensitivity for the same conditions. Using an average of five sodium signals for this distilled demineralized water and extrapolating to $S/N = 2$, the LOD of 2 ng/L is obtained. This shows a significant improvement over the previous result (*11*) of 30 ng/L. The magnitude of this improvement is reasonable for the increase in modulation frequency from 800 Hz to 150 kHz, although it was not possible to make a direct comparison of the performance of this system at the two frequencies because of the low frequency limit on the lock-in amplifier. Other modulation frequencies between 150 kHz and 1 MHz were investigated, but no substantial improvement was seen above 150 kHz.

It is encouraging that this improvement in detection limit was achieved even though only moderate laser powers were used. As shown in Figure 7, the dispersion signal, S_D, for residual sodium present in distilled demineralized water at approximately 2 ppb is roughly proportional to P^2 over the range of powers used here. Since our power levels are not at the saturation limit, and because N_{hop} is roughly proportional to P, further improvements in S/N and LOD can be expected as the laser power is increased.

Conclusions

High-frequency modulated polarization spectroscopy provides detection limits for sodium that compare favorably with those of other atomic methods such as atomic fluorescence and graphite furnace atomic absorption. Although the signal in polarization spectroscopy is very

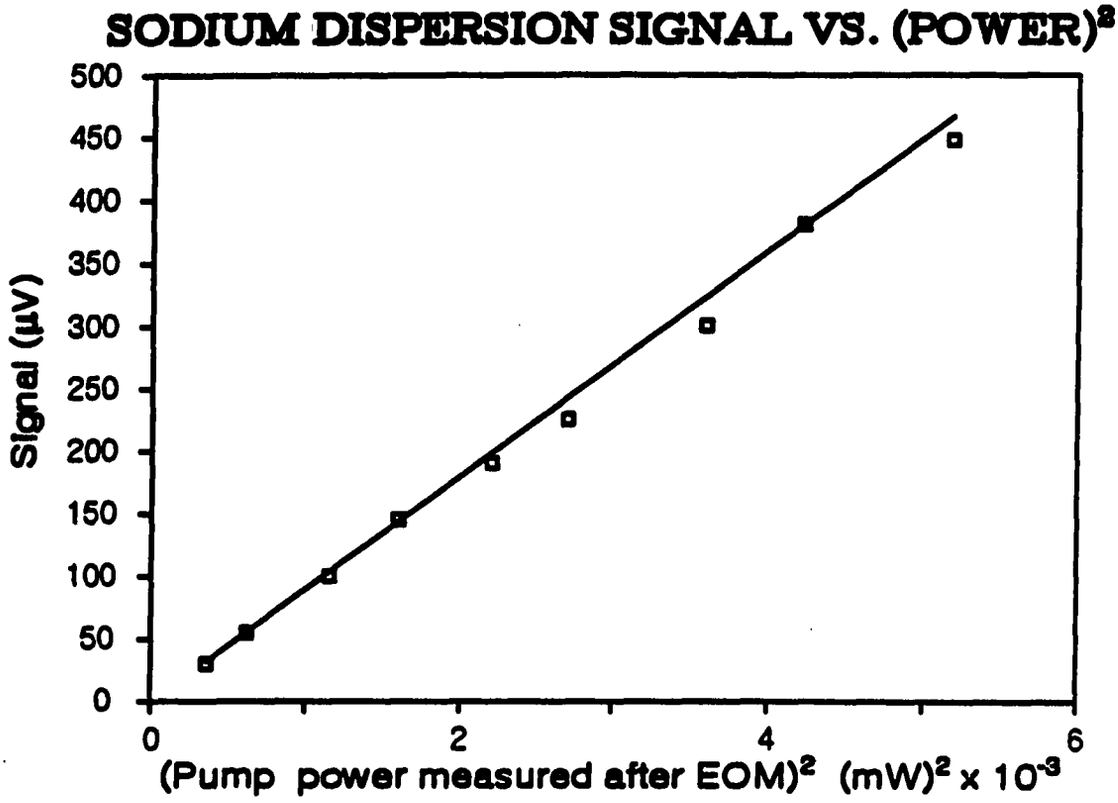

Figure 7. Quadratic dependence of dispersion signal on laser power
Sample is distilled demineralized water with residual sodium concentration of approximately 2 μg/L (ppb).
EOM designates the Pockels cell electrooptic modulator.

small, the method of polarization modulation and lock-in detection allows for good *S/N* levels by reducing the effects of background. Modulation of the polarization of the pump beam gives an advantage over simple amplitude modulation because there is no "off" cycle. Hence, the scattered background light is better rejected by phase sensitive detection with polarization modulation. This technique is ideally suited for highly luminous or highly scattering environments. Polarization spectroscopy has similarities to coherent forward scattering (CFS), which uses a magnetic field to induce anisotropy in the sample. However, the LOD for sodium obtained here is four orders of magnitude lower than that reported for laser-excited CFS (*26*). The signals here are larger and the noise levels are lower. In conclusion, the detection power of polarization spectroscopy for elemental analysis has been substantially improved by using high-frequency modulation to reduce the effects of laser flicker noise so that advantage can be taken of the larger dispersion signal and its straight-forward linear relationship with concentration.

CHAPTER III. FLUORESCENCE-DETECTED CIRCULAR DICHROISM FOR ON-COLUMN DETECTION IN CAPILLARY ELECTROPHORESIS

Introduction

Many of the current challenges facing developmental analytical chemists arise from the rapidly advancing and expanding fields related to biology and medicine. The need for improved analytical separation and detection methods, especially those suitable for complex biochemical systems, is increasing (*27-29*). In the area of separations, the move has been toward smaller diameter chromatographic columns (*30, 31*). Capillary chromatography and capillary electrophoresis (CE) are now offering highly efficient and versatile separations (*32*).

On the detection side, a number of well known methods have been modified for increased sensitivity and applied to these separation techniques. Some methods such as conductivity (*33, 34*) and indirect fluorescence (*35, 36*) are essentially universal. The best reported detection limits, given as quantity injected, for these techniques are approximately 500 fmol (*34*) and 50 amol (*36*), respectively. However, in complex biological samples a detection method with additional selectivity can be advantageous. Since many biomolecules are inherently chiral, it is reasonable to look toward methods that take advantage of the specificity arising from optical activity. Fluorescence-detected circular dichroism (FDCD), first described by Turner et al. in 1974 (*37*), is one such method.

In addition to high selectivity, the inherent chirality information of FDCD is an advantage over many commonly used detection methods.

Chiral molecules may exhibit circular dichroism (CD) that varies in relation to molecular conformation. Since FDCD measurements can be directly related to standard CD measurements (*37-39*) they can provide the analyst with important structural information. This type of information is potentially useful for determining enantiomeric composition, monitoring the progress of a reaction, or comparing the effects of different solvents upon conformation.

Optical rotation is another method which can provide this type of structural information for chiral molecules. A laser-based micropolarimeter (*3*) has been introduced as an optical activity detector (OAD) for liquid chromatography and demonstrated in the analysis of a variety of samples (*40-45*). One system employing high-frequency modulation (*13*) can measure rotations as small as 10^{-6} degree, which corresponds to detectability of approximately 1 ng or 10^{-7} M for favorable analytes. Modifications to the polarimeter have enabled its coupling to microbore LC (*46*), but further miniaturizations are not likely to produce a polarimetric detector suitable for capillary columns smaller than 200-μm i.d. Further improvements in the OAD and application to very small volumes are also hindered by the signal dependence on path length. Thus, it does not readily lend itself to on-column detection, and other methods capable of measuring optical activity need to be explored for capillary systems.

The potential information content of FDCD is further increased by the ease with which total fluorescence (FL) can be measured simultaneously. In this way, it may be possible to actually identify a

compound based on its unique FDCD/FL signal ratio, as was shown in an analogous manner for PTH amino acids (*47*) using optical rotation and ultraviolet absorbance (OA/UV) measurements. Likewise, determination of enantiomeric purity, which is especially important in the pharmaceutical industry, may be possible with the FDCD/FL measurement, as has been shown for OA/UV and OA/RI (refractive index) methods (*43*, *48*).

Because of the ease of miniaturization and high sensitivity, direct fluorescence analysis is especially suited to detection in CE. Sub-attomole detection limits have recently been reported for direct fluorescence of derivatized amino acids in capillary electrophoresis. Kuhr and Yeung reported a detection limit of 0.5 amol for dansyl-alanine (*36*), and Cheng and Dovichi reported 0.009 amol as the detection limit for a better-matched chromophore, the FITC (fluorescein isothiocyanate) derivative of alanine (*49*). FDCD is a variation of fluorescence detection and is therefore also readily interfaced to CE.

Previously, Synovec and Yeung developed a system for FDCD detection in HPLC (*25*) which used a postcolumn flow cell with a 1.2-cm observation path length and 14 μL total volume. Although this FDCD-HPLC system achieved an improved limit of detection (LOD) for riboflavin (170 pg) based on a chiral method, it also revealed troublesome artifact signals. The artifacts were demonstrated by the substantial FDCD signal obtained for an optically inactive sample component, 4-methylumbelliferone. The artifact is attributed to imperfections in the circular polarization of the incident light and has been discussed in several papers (*39*, *50*, *51*). Although such artifacts do not necessarily reduce

the detection power of FDCD, they do reduce the selectivity of the technique and complicate quantitation. Several approaches for reducing the non-CD artifact have been suggested (*37*, *39*, *50*, *51*), but only limited success has been demonstrated.

Capillary electrophoresis, first introduced as high-performance zone electrophoresis (HPZE) (*33*) and capillary zone electrophoresis (CZE) (*52*, *53*), has rapidly come to the forefront in analytical chemistry as a very promising technique for the separation of charged species. This is substantiated by recent reviews (*54-56*). Capillary internal diameters typically range from 5-100 μm, and detection volumes can be few to tens of picoliters. The current surge of activity in molecular biology and biotechnology (*32*, *57*, *58*) and the potential applications of CE involving analytically interesting biomolecules make a strong argument for coupling the separation with FDCD detection. The objective of the work described below is to demonstrate the successful application of on-column FDCD in CE and to show improved limits of detection and better discrimination of artifact signals.

Experimental

Electrophoresis apparatus

The electrophoresis system used in this work is very similar to one described previously (*36*) and is shown in Figure 8. A high voltage power supply (Spellman, Plainview, NY, Model UHR50PN50) provides the electromotive force across the capillary. Each end of the capillary is immersed in a buffer solution containing electrodes made of Chromel P wire. The injection end of the capillary is in electrical contact with

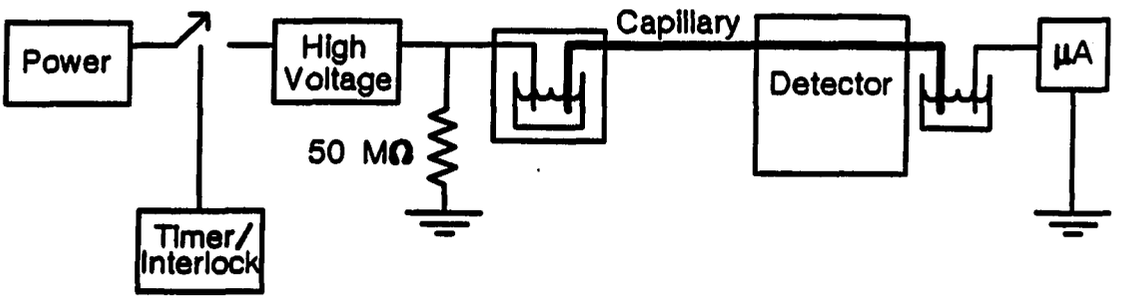

Figure 8. Capillary electrophoresis system

the high voltage lead of the power supply, while the detector end is held at ground potential. Measurement of the voltage drop across a 10-MΩ resistor in the ground return line allows convenient monitoring of current passing through the capillary. The anodic, high voltage, lead is isolated in a polycarbonate box equipped with a safety interlock. A timer circuit is incorporated into the interlock circuitry to allow control of electromigration injection times. A 50-MΩ load resistor is included in the circuit parallel to the capillary, from anode to ground, and acts as a current shunt.

Capillary columns

A variety of fused silica capillaries (10-25 μm i.d., 150 μm o.d., 50-80 cm in length; Polymicro Technologies, Phoenix, AZ), both untreated and silylated, were used in this work. The silylation procedure employed here was a modification of a method originally described for the silylation of glass plates (*59*, *60*). The columns were first rinsed with acetone to remove impurities and then filled with a 0.2% solution of γ-(methacryloxy)-propyltrimethoxysilane (Sigma, St. Louis, MO) in a 1:1 (v/v) ethanol/water solvent mixture. These filled capillaries were heated to 60 °C for 45 minutes to increase the extent of reaction and evaporate excess silane. Finally, the capillaries were rinsed with methanol, filled with buffer solution, and equilibrated in the electrophoresis system.

A 1-cm section of the polyimide coating on each capillary was burned away under a gentle flame to create a suitable detection region approximately 10 cm from the cathodic end. In some cases a small

section of this coating was also removed from the injection end of the column to minimize any trapping of analyte near the entrance of the capillary.

FDCD detection system

A schematic diagram of the detection system, which has similarities to the earlier system (*25*) is shown in Figure 9. An argon ion laser (Control Laser Corp., Orlando, CA, Model 554A) operating at 488 nm is the excitation source. The linearly polarized laser light is converted into alternating left and right circularly polarized light (LCPL, RCPL) by a Pockels cell electrooptic modulator (Lasermetrics Inc., Teaneck, NJ, Model 3030) as described in Chapter II and elsewhere (*61*).

The modulated light is focused onto the detection region of the capillary by a short focal length lens, and collection of fluorescence is at 90° to the incident beam with a 10× microscope objective. An enlarged image of fluorescence from within the capillary is focused on the photomultiplier tube (PMT) (Hamamatsu, Middlesex, NJ, Model R928). Two sets of spatial filters and color filters (Corning Glass, Corning, NY, Model 3-70) are mounted in a blackened tube before the PMT to selectively pass fluorescence while rejecting scattered laser light and room light. Earlier work in indirect fluorescence detection with capillary electrophoresis (*35*, *36*) had the column mounted for Brewster's angle of incidence to minimize scattering. However, in FDCD it is necessary to preserve the circular polarization purity inside the column, and the Brewster's angle arrangement is not suitable. Therefore, the column is mounted for normal incidence in these

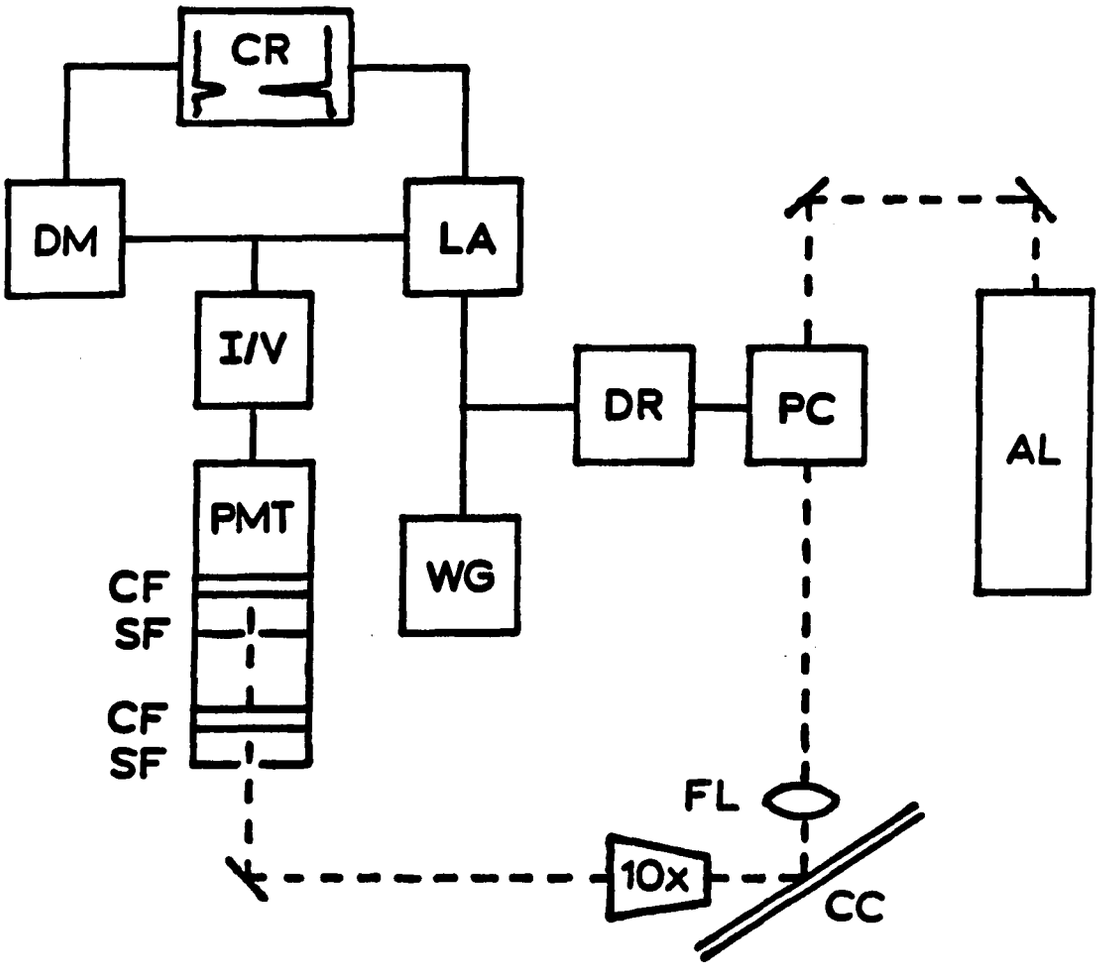

Figure 9. Schematic diagram of FDCD and FL detection system for capillary electrophoresis
(AL) Argon Laser, (PC) Pockels Cell, (DR) Driver, (WG) Waveform Generator, (LA) Lock-in Amplifier, (DM) Digital Multimeter, (CR) Dual-pen Chart Recorder, (FL) Focusing Lens, (CC) Capillary Column, (10x) Microscope Objective, (SF) Spatial Filters, (CF) Color Filters, (PMT) Photomultiplier Tube, (I/V) Current-to-Voltage Converter. Solid lines indicate electrical connections and dashed lines show the optical path. The capillary axis is perpendicular to the incident beam and makes an angle of about 30° with the direction of collection.

experiments. When properly focused, all light rays will enter perpendicular to the cylindrical cell, thereby preserving the circular polarization. The angle between the column and the collection optics can be adjusted (*62*) to minimize the amount of scatter collected while retaining normal incidence at the capillary.

The fluorescence signal from the PMT is converted to a voltage by a 10 kΩ resistor and sent to the lock-in amplifier (EG&G PARC, Princeton, NJ, Model HR-8) and a digital multimeter (Keithley Instruments, Cleveland, OH, Model 160B) simultaneously. The demodulated FDCD signal is obtained from the lock-in amplifier using a 1-s time constant, and the digital multimeter displays the average total fluorescence signal. Both of these signals are displayed on the dual-pen chart recorder (Measurement Technology Inc., Denver, CO, Model CR452).

Reagents and samples

All chemicals were certified grade unless specified otherwise. Sodium bicarbonate (Fisher Scientific, Fair Lawn, NJ) buffers were prepared in deionized water (Millipore Corp., Bedford, MA, Milli-Q System) and pH-adjusted with sodium hydroxide solution. Standard samples of (-)-riboflavin (Aldrich Chemical, Milwaukee, WI, 98%) and disodium fluorescein (Eastman Kodak, Rochester, NY) were dissolved in the electrophoretic buffer solutions employed. Fluorescein was also included in some of the buffer systems. Because these experiments were carried out in basic solution (pH 8.5-10.5), buffers were purged with nitrogen before use and the pH was checked or adjusted on a daily basis. All quantitative data were obtained with freshly prepared buffer and

sample solutions. Figure 10 shows the structures of the two test compounds used in this work: optically active riboflavin and optically inactive fluorescein.

Operating procedures

In the studies reported here, the argon laser is under servo control for power stability and provides between 150 mW and 300 mW at the capillary. Unless otherwise specified, LCPL and RCPL are modulated at 1 kHz. The modulation electronics are optimized for balance and efficiency (typically 90%) before making any fluorescence measurements. Optimal positioning of the capillary requires fine two-dimensional adjustment and is characterized by good beam quality in the transmitted beam. Initially the electrophoresis buffer contains a low concentration of disodium fluorescein (10^{-5} to 10^{-6} M) to aid in alignment of collection optics. The total background fluorescence signal for these buffers is kept in the 2–5-μA range by adjustment of the PMT voltage (200–700 V).

The major buffer component is sodium bicarbonate at approximately 1×10^{-3} M. All injections are by electromigration, typically 1 s at +30 kV, and the voltage is held constant at +30 kV throughout each run. Simultaneous FDCD and FL electropherograms are obtained for all samples injected. Calculations are based on peak heights and peak-to-peak noise measured from the recorded electropherograms.

Riboflavin

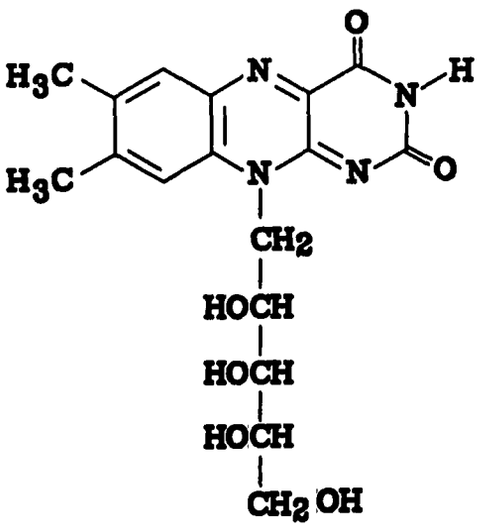

Fluorescein

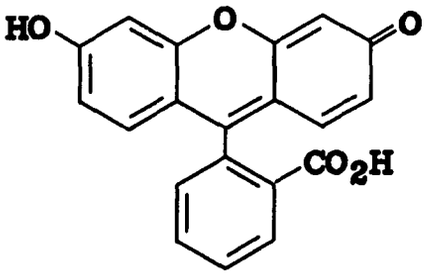

Figure 10. Molecular structures for the fluorophores riboflavin (optically active) and fluorescein (optically inactive)

Results and Discussion

Feasibility

It is first necessary to show that FDCD is feasible as a detection method in open tubular capillaries of typical CE dimensions. With this as our aim we chose to use a simple electrophoretic separation and did not necessarily optimize the CE system for highly efficient separations. Because the balance between incident intensity for LCPL and RCPL ($I_{0,L}$ and $I_{0,R}$) and the stability in the modulation are very critical for CD measurements (*25*), routine stability measurements are made to assess system performance. The fluorescence signal produced as fluorescein flows through the capillary provides the data for this measurement. Stability is calculated as $\frac{1}{2}(I_F/N)$, where I_F is the total fluorescence signal from the phototube, measured as voltage after conversion, and N is the noise on the lock-in baseline.

A stability of 5000 is routinely obtained in this system. Greater stability (1×10^4) was seen for larger diameter columns under gravity-flow or compressed-gas-pressure flow, and stabilities as high as 1×10^5 have been measured for the incident light and for the laser light transmitted through the capillary. The stability measured for fluorescence is typically 10 times worse than that of the incident light. It is also expected that stability will decrease as the capillary dimensions become smaller due to increased restraints on alignment and mechanical rigidity. In addition, complications such as heating the analyte or bleaching its fluorescence will become more severe and limit stability as the laser is focused into smaller volumes. Considering

these factors, a stability of 5000 is still quite reasonable, and FDCD signals for 5×10^{-5} M riboflavin can be easily obtained.

In some ways, FDCD seems better suited to CE separations than to high-performance liquid chromatography (HPLC). Optimization of modulation and detection requires that the analyst be able to change the composition of eluting buffer rapidly and with relative ease. It is also important that this procedure not alter the optical alignment or any other experimental parameters that can affect the balance between $I_{0,L}$ and $I_{0,R}$. In the HPLC system (*25*) it was necessary to connect a second eluent pump to the detection cell in order to introduce an optically inactive fluorophore for the purpose of balancing I_0. In CE, it is very simple to change the migrating buffer. The injection end of the capillary is simply inserted into another vial containing the new buffer, just as when a sample is injected. The reequilibration of the column and fluorescence signal following a buffer change is rapid in comparison to HPLC, and switching buffers does not disturb the precise alignment or alter the polarization modulation. In addition, the methods developed here for assessment of stability and for continuous monitoring of direct fluorescence make FDCD more attractive because they do not require any changes in the optical system.

Both untreated and silylated columns worked well in these studies. It is expected that the untreated columns would start to show reproducibility problems at the pH values used here since silica is known to deteriorate at pH values greater than 8. However, some untreated columns were used for several weeks and showed no signs of this problem.

In the analysis of proteins by CE (*63*) deactivation of the silica surface is necessary. Fortunately, FDCD is compatible with these modifications of the inner capillary surface.

Discrimination of artifacts

Actual verification that stability is sufficient can only be seen in the FDCD results. Figure 11 shows the FDCD and FL electropherograms for a sample containing riboflavin and fluorescein. The lower traces correspond to direct fluorescence while the upper traces show the FDCD signal. Under these separation conditions, riboflavin is the first component to migrate past the detector region. A second optically active peak which migrates slower than riboflavin is apparent in these traces. This peak has been attributed to a photodecomposition product of riboflavin since it is not present in freshly prepared solutions but begins to appear in solutions at pH 9.3 after a few hours of exposure to light. Fluorescein is the slowest migrating peak in these experiments. Figure 11 shows that good separation efficiencies are obtained. The 1-s injection time and the 120-s migration for riboflavin limit the number of available theoretical plates to 57,600, calculated as $N = 4(t_R/W_{\frac{1}{2}})^2$. We measured 80,000 theoretical plates for riboflavin and even more for fluorescein in Figure 11. This is in good agreement with predictions since the injected plug is probably not square.

Because fluorescein is not optically active, it cannot produce a true FDCD signal. However, as seen previously (*25*), and as evident in the first trace in Figure 11, there is some FDCD signal associated with the optically inactive species. A ratio of merit (discrimination or

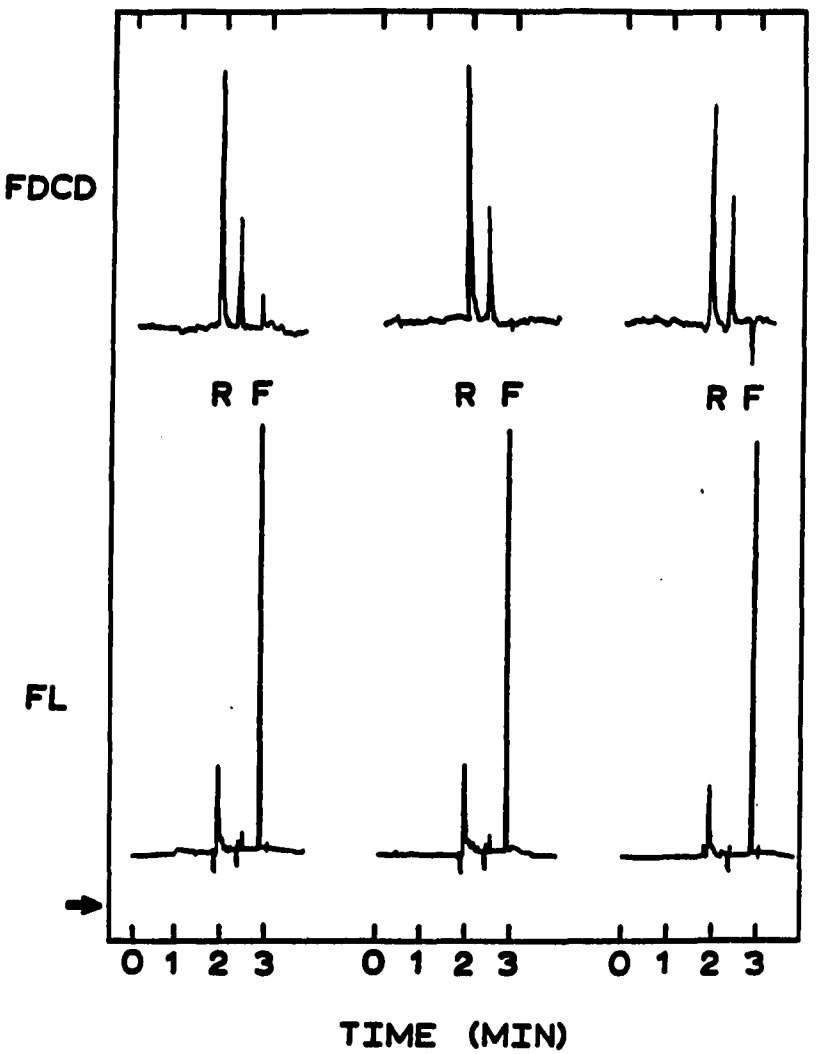

Figure 11. Control of artifact suppression with adjustment of Pockels cell bias voltage for a series of simultaneous FDCD and FL electropherograms
Sample: 4×10^{-5} M riboflavin (R), 6×10^{-6} M fluorescein (F). Buffer: 2×10^{-3} M bicarbonate, 2×10^{-6} M fluorescein, pH 9.3. Column: 20 μm i.d. × 50 cm, untreated. The arrow on the FL scale indicates the baseline level when fluorescein is absent from the running buffer.

suppression ratio) can be calculated directly from these simultaneous measurements for comparison of artifact suppression. We define this ratio, r, as

$$r = \frac{FDCD_{(oi)}/FL_{(oi)}}{FDCD_{(oa)}/FL_{(oa)}} \qquad (7)$$

where *FDCD* is the fluorescence-detected circular dichroism signal, *FL* is the direct fluorescence signal, and (oi) and (oa) indicate optically inactive and optically active samples, respectively. As long as FDCD and FL signals are obtained simultaneously for both active and inactive species, comparison of r values for a given optically active analyte will be valid, even if other experimental parameters vary.

In Figure 11 the concentration of fluorescein is selected to produce a FL signal much larger than the riboflavin FL signal in order to emphasize the degree to which the non-CD artifact is suppressed. This series of electropherograms is obtained by varying the relative amounts of incident LCPL and RCPL by adjusting the bias voltage on the Pockels cell driver. This shows how very small changes in modulation can dramatically affect the suppression of artifacts while the riboflavin FDCD signal changes very little. Similar effects are seen if the lock-in amplifier phase is changed slightly to either side of the optimum phase. In the FDCD-HPLC system (*25*), the r value is calculated to be +0.55. The r values for the three traces in Figure 11 (left to right) are +0.03, -0.007, and -0.03. This demonstrates the ability to

substantially reduce and essentially eliminate these artifacts with the FDCD-CE system.

We had originally hoped that by placing fluorescein in the buffer solution, the stability could be continuously monitored and adjustments made to maintain good suppression. However, we discovered that it was just as simple to inject a plug of fluorescein only when it was necessary to see the fluorescent image, to measure stability, or to set the driver bias for balance of I_0. Removal of fluorescein from the buffer also led to improved signal-to-noise (*S/N*) by eliminating background fluorescence signal.

Precision and stability of the optical alignment are very critical in achieving and maintaining a good discrimination level. We frequently observed drifting in the degree of discrimination. Artifacts that had once been suppressed would reappear after several minutes without any operator intervention. These changes may be caused by electronic instability in the modulation driver or temperature changes in either the electronic components or in the Pockels cell crystal. Micro-scale mechanical movement of optical components (e.g., the capillary detection region) could also lead to a significant imbalance in the polarization modulation resulting from changes in surface reflections and strain-induced birefringence.

These difficulties point to areas of improvement for the FDCD-CE technique. The Pockels cell requires relatively large modulated voltages and is also temperature sensitive. A photoelastic modulator (PEM) device can produce alternating LCPL and RCPL with moderate power

input (*5*) and should exhibit long-term stability due to its inherent periodicity. The PEM also has a much larger angular aperture than the Pockels cell which makes it easier to align. In addition, mounting of the capillary detection region should be more rigid to reduce mechanical vibration.

Another example of artifact suppression for a mixture of riboflavin and fluorescein is shown in Figure 12. In this case, the ratio of fluorescein to bicarbonate in the buffer solution has been increased 10-fold. This causes the riboflavin band to displace a larger fraction of fluorescein in the buffer. Since riboflavin is a much weaker fluorophore than fluorescein at the wavelength used here, this displacement results in a negative-going FL peak for riboflavin, similar to the peaks seen in indirect fluorescence detection (*35, 36*). Interestingly, the FDCD trace is unaffected because ΔI_F is derived only from the riboflavin molecules, and the background fluorescence shows no optical activity. This further supports the selectivity of the FDCD method.

Limit of detection

To estimate the quantity injected, Q, we use

$$Q = l \cdot A \cdot C \qquad (8)$$

as given by Lukacs and Jorgenson (*64*), where l is the length of the sample plug introduced, A is the cross-sectional area of the column, and C is the concentration of analyte in the sample solution. Since we perform electroinjection and separation at the same applied voltage l is calculated as injection time multiplied by the linear flow rate.

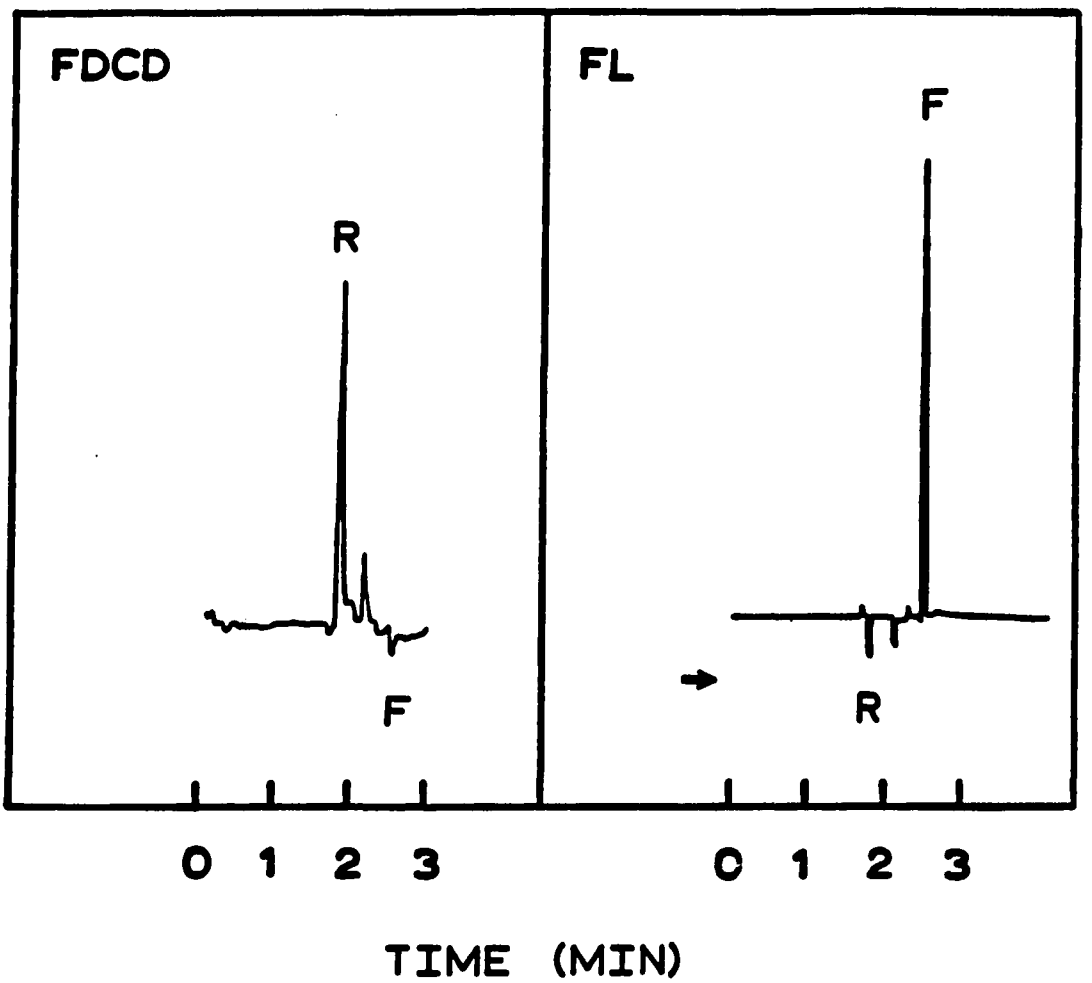

Figure 12. Simultaneous FDCD and FL electropherogram showing negative FL signal for riboflavin due to displacement of fluorescein in buffer solution
Sample: 1×10^{-4} M riboflavin (R), 5×10^{-5} M fluorescein (F).
Buffer: 1×10^{-3} M bicarbonate, 1×10^{-5} M fluorescein, pH 9.3. Column: 20 μm i.d. × 50 cm, untreated. The arrow on the FL scale indicates the baseline level when fluorescein is absent from the running buffer.

Linear flow rate is determined from the time required for the analyte to migrate from the inlet to the detector. This method likely overestimates the quantity injected because the power supply does not produce 30 kV instantaneously. A previous paper (*36*) discusses the injection plug profile for a similar CE system. The results of that study indicate that a 1-s injection at 30 kV produces a plug that is triangular in shape. To compensate for this, we divide *Q* from equation 8 by 2 to obtain the injected quantity. The injection volume is calculated to be 0.8 nL for a 1-s, +30-kV injection of riboflavin solution in 2×10^{-3} M bicarbonate buffer at pH 9.3 in an untreated 20-μm-i.d. column and 0.2 nL in a 10-μm silylated column under similar conditions.

Although the artifact signals here are usually small, all FDCD signals are corrected for any artifact prior to other calculations. The corrected FDCD signal, *FDCD'*, is given by

$$FDCD'_{(oa)} = FDCD_{(oa)} - \frac{FDCD_{(oi)}}{FL_{(oi)}} \times FL_{(oa)} \qquad (9)$$

where all terms are defined above and the sign of FDCD artifact is taken into account.

The best FDCD LOD (*S/N* = 3) achieved for riboflavin is 0.2 fmol (0.07 pg), as calculated from the corrected FDCD signal of 45.5 units (90 μV), and the FDCD baseline noise of 0.3 unit (0.6 μV). The concentration LOD is 1×10^{-6} M injected. This result is obtained for a 0.2-nL injection of a solution containing 5×10^{-5} M riboflavin and

7×10^{-6} M fluorescein in a 10-μm-i.d. silylated column. The electrophoretic buffer, 2×10^{-3} M bicarbonate at pH 9.3, contains no fluorescein. This detection limit shows more than a 2000-fold improvement over the FDCD-HPLC system (*25*). Also important for consideration is the dynamic range of the system. We found that in general the analyte concentration has to be lower than that of the running buffer by a factor of 10 to preserve the separation efficiency. This then provides a dynamic range of 200 in the present experiment. Naturally, higher buffer strength can be used (which in general is better for CE) to extend the dynamic range. Since the buffer is nonfluorescing, the detection limit should not change, in contrast to the case of indirect fluorescence detection (*35*, *36*).

Several differences between the FDCD-HPLC system (*25*) and this FDCD-CE system are worth noting. The wavelength used in the earlier system was 325 nm and is more favorable than 488 nm for riboflavin absorption. Also, the previous system used a 150-kHz modulation frequency and a 10-s time constant, compared to a 1-kHz modulation and a 1-s time constant used here. We found it difficult to achieve the high degree of artifact discrimination at the higher frequencies, which may indicate that the Pockels cell driver becomes less stable as frequency increases. Despite the disadvantages associated with these factors, the reduced column diameter and detection volume in CE and the use of an imaging system with better stray light rejection allow improvement in the FDCD detection limit.

Conclusions and Future Directions

The ability to measure optical activity in such a small quantity has obvious applications in biological fields, where sample quantities are often limited. The technique can be applied to a wide variety of analytes including derivatized amino acids, peptides, and proteins. The very rapid separation (<2 min) of several NDA amino acids by CE (*65*) has recently been demonstrated. Even though all amino acids could not be separated with this method, simultaneous FDCD/FL detection of these amino acid derivatives using a helium cadmium (442 nm) laser may allow identification for implementation in protein sequencing, where the increased speed of analysis would be of great advantage. McCormick (*63*) has shown highly efficient separations of proteins and peptides in modified capillaries. By use of the UV lines of an argon ion laser, the natural fluorescence of tryptophan (and tyrosine) should allow FDCD analysis for these types of separations. The application of such an FDCD-CE system for the analysis of protein components from a single cell is also of interest. Even when chiral species are separated in CE (*66, 67*), FDCD will allow identification of the migration order of the enantiomers.

To our knowledge, this work demonstrates the measurement of an optical activity signal for the smallest volume and smallest absolute quantity of any chiral species. Fluorescence-detected circular dichroism will never be as sensitive as direct fluorescence because the signal is derived from $\Delta\epsilon$ rather than ϵ, and $\Delta\epsilon$ is typically orders of magnitude smaller than ϵ. Thus, FDCD trades some sensitivity for the

increase in selectivity. The fact that fluorescence, indirect fluorescence, and FDCD analyses can all be done with the same apparatus and applied to the minute volumes typical of capillary electrophoresis and capillary chromatography should lead to increased use of these techniques, both in combination and separately.

CHAPTER IV. REFINEMENTS IN FDCD/FL-CE AND PRELIMINARY ANALYSIS OF AMINO ACIDS

Introduction

In Chapter III we demonstrated the feasibility of simultaneous on-column detection in capillary electrophoresis (CE) by fluorescence-detected circular dichroism (FDCD) and direct fluorescence (FL). Although discrimination of non-CD artifacts was substantially improved over earlier work, achieving reproducibility in discrimination proved difficult. Labor intensive trial-and-error adjustments of optics and detection electronics were necessary to obtain suitable discrimination levels. The tendency for the discrimination to drift with time presented further complications. Before we can substantiate greater potential usefulness of FDCD in the analysis of important biological molecules, refinements in the optics and electronics of the FDCD detector are needed. More routine optimization and operation is required to achieve satisfactory precision and accuracy by FDCD. In this chapter we describe several instrumental improvements and report the first analysis of derivatized amino acids by FDCD/FL-CE.

The analysis of amino acids for protein sequencing has been routinely accomplished for many years by the Edman degradation scheme (*68*). In the typical Edman procedure, the N-terminal amino acid is derivatized with the chromophoric reagent phenyl isothiocyanate (*69*). The phenyl thiocarbamyl (PTC) amino acid residue is then cleaved from the protein or peptide by acid hydrolysis and recovered by extraction as the phenyl thiohydantoin (PTH) derivative. This PTH derivative is then

identified chromatographically. Gradient elution liquid chromatography in the reversed phase mode with UV absorbance detection is the most common method of identification, although gas chromatography (GC) and thin layer chromatography (TLC) have also been used. This process is repeated for each subsequent amino acid in the chain. The overall sequencing procedure has been automated but continues to be time consuming. Positive identification by liquid chromatography requires lengthy separation times with gradient elution and additional time for reequilibration to initial column conditions before the next injection. Commercially available sequencers require mg quantities of protein to obtain complete sequence information. The minimum sample requirement depends on extraction efficiencies as well as LC detection limits, which currently are at the pmol level (*70*) for standard systems.

Recent advances in molecular biology and peptide and protein synthesis have led to an increased need for more rapid and more sensitive sequencing schemes. Chan and Yeung (*47*) described a method of amino acid identification based upon a 10-minute isocratic HPLC separation of PTH-amino acids with simultaneous detection by optical activity (OA) and UV absorbance. Although the OA/UV ratio alone did not positively identify all 20 common PTH-amino acids, the differences in chirality of the individual amino acid derivatives were sufficient to allow identification when isocratic separations were performed at two different pH values and both the retention time and the OA/UV response were considered. In a sequencing scheme, it is not mandatory that the chromatographic method be capable of separating all possible amino acids

simultaneously, because only one amino acid is cleaved and injected during each step. The detector only needs to distinguish those amino acids which would coelute. Thus, a detector with increased specificity can decrease the time required for separation and thereby speed the sequence analysis.

Because FDCD and FL detection probe the same molecular and electronic properties that give rise to OA and UV signals, respectively, it may be feasible to pursue amino acid identification by FDCD/FL detection. The suitability of FDCD and FL to open tubular columns of 10-50 μm i.d. (*71*) provides the advantage of much lower mass detection limits than those obtained by conventional LC (*25*). In addition, the demonstrated compatibility of FDCD and FL with capillary electrophoresis gives potential for very rapid separations of derivatized amino acids (*61, 72*) without gradient complications. If micro-scale Edman degradation reactions using a fluorescent tag molecule (*70*) become more routine, then FDCD/FL-CE may present the most rapid, sensitive, and simple identification method in protein sequencing. It is advantageous to determine amino acid sequence by two or more complementary techniques (*70*). Rapid sequence analysis using CE as a second technique could improve the accuracy and thereby increase confidence in the results derived from a sequencing experiment.

Because of the potential applications in protein sequencing, we are particularly interested in investigating FDCD of amino acids. Unfortunately, few of the common amino acids (tryptophan, tyrosine, and phenylalanine) have appreciable intrinsic fluorescence. Therefore,

FDCD analysis requires derivatization of the amino acids with a fluorescent tag molecule. Many tagging reagents have been developed specifically for fluorescence analysis of amino acids (*73*, *74*) providing highly fluorescent derivatives. The usefulness of a particular tag in FDCD, however, depends on two additional criteria. The derivatization reaction conditions and mechanism must preserve the chirality (i.e., prevent racemization), and the tag chromophore must interact strongly enough with the optically active center to exhibit circular dichroism.

Although a number of amino acid derivatives show optical activity as measured by specific rotation (*47*), it is difficult to predict whether the attached chromophore will sense the asymmetric environment and display circular dichroism. CD spectra of proteins are commonly used to characterize conformational changes that occur on binding of a fluorescent tag molecule (*75-78*), but induced chirality in an achiral tag molecule is less commonly observed. Often the magnitude of induced CD in a tag molecule decreases substantially as the distance between the tag chromophore and the asymmetric center increases (*79*), but other factors may also be important.

In the present work, fluorescein isothiocyanate (FITC) was chosen as the chromophoric derivatizing agent for amino acids for several reasons. Most importantly, the retention of optical activity in amino acids after derivatization with FITC has been reported (*80*, *81*) giving reasonable assurance that racemization does not occur in the reaction process. In addition, Mercola et al. (*82*) observed substantial induced

optical activity of FITC bound to insulin by measuring CD from 450 to 550 nm. Another group measured induced optical activity in FITC-myoglobin by CD near 280 nm (*76*). These references give evidence that optical activity can be retained upon derivatization with FITC. Furthermore, FITC derivatives are highly fluorescent and suitable for excitation by either an argon ion or helium cadmium lasers (*83*). Also important is the fact that the isothiocyanate group reacts with both primary and secondary amine groups on the amino acids (*80, 84*). The reaction proceeds more slowly for trifunctional amino acids, but all the protein amino acids can be derivatized by FITC. The procedure is straight forward and reaction occurs quickly.

This derivatization can be carried out in high pH aqueous solutions which are compatible with CE separations. The methodology is similar to the phenyl isothiocyanate (PITC) reactions used in the Edman degradation procedure and is therefore easily incorporated into a protein sequencing scheme. Sequencing has already been demonstrated by Kawauchi and coworkers using FITC derivatization with identification by TLC (*85*) and by gradient HPLC (*86*). The conventional HPLC method still requires time consuming gradient elution, but subpicomole injected quantities of the FTH-amino acids can be detected by direct fluorescence.

The reaction of FITC with amino acids is proposed as a two-step process (*87*) as shown in Figure 13. The most common form of FITC is fluorescein-5-isothiocyanate (also called FITC-I), which has the isothiocyanate group attached at the 5-position of the fluorescein

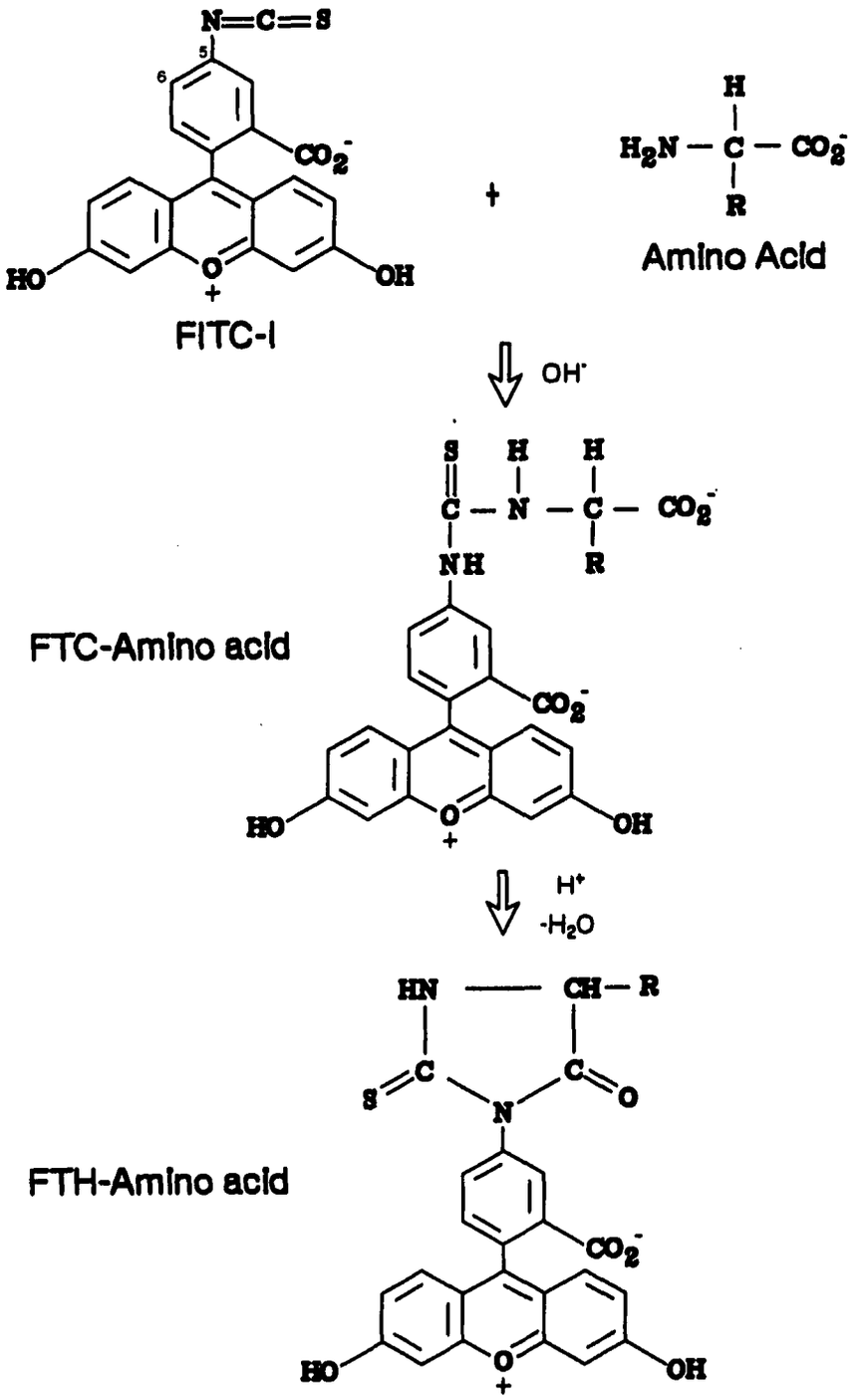

Figure 13. Proposed reaction of amino acids with fluorescein isothiocyanate (FITC) to form the fluorescein thiocarbamyl (FTC) and fluorescein thiohydantoin (FTH) derivatives

structure as shown in this figure. The other common form of FITC, fluorescein-6-isothiocyanate (also called FITC-II) has also been used for derivatization of amino acids. The reaction is identical to the one shown here except that attachment of the isothiocyanate is at the 6-position. In basic solution the amino acid and FITC combine to produce the fluorescein thiocarbamyl (FTC) derivative. If strong acid is added after this step, the derivative is converted into the cyclic fluorescein thiohydantoin (FTH) amino acid. Optical activity is reported for both the FTC (*80*) and FTH (*81*) amino acids, but undesirable side reactions can occur under the strongly acidic conditions necessary to form the latter. Since we desired a simple reaction procedure yielding an optically active fluorophore for evaluation of the FDCD method, we chose to use the FTC-amino acids in this work.

Experimental

Electrophoresis system

With the exception of the components noted below, the electrophoresis system employed here is identical to that described in Chapter III. (See Figure 8, page 41.) The high voltage power supply (Beta Electric) has maximum output of +30 kV and 2 mA. A 20-MΩ parallel load resistor was assembled by series connection of ten 2-MΩ high voltage resistors (Victoreen, MOX-5-12), each rated for operation up to 37 kV and 12 W. Since the buffer-filled capillary has resistance in the Gigaohm range, the equivalent resistance for the parallel combination of capillary and load resistor is nearly 20 MΩ. At the maximum voltage (+30 kV) the maximum current drawn from the supply is limited to 1.5 mA.

This prevents a current limiting situation which would reduce the maximum voltage delivered by the power supply. The resistor assembly is housed in a ventilated plastic box which provides electrical safety for the operator and allows for heat dissipation.

For convenience, the electronic timing and interlock circuit was omitted in the new system. Injections were carried out by electromigration for approximately one second at the running voltage, which was typically +28 kV. Although the injection times could not be precisely controlled, the simultaneous monitoring of direct fluorescence signals provided a convenient means of assessing the reproducibility of injections and making comparisons of relative amounts injected.

Capillary columns and mounting of detection region

Fused silica capillary columns (Polymicro Technologies, Phoenix, AZ) of 20 to 50 μm i.d. and approximately 70 cm in length were pretreated by rinsing first with methanol and then with 0.1 M NaOH before filling with buffer solution. No alteration of the capillary inner surface was used in these studies.

Modifications were made in the procedure for mounting the capillary detection region so as to improve mechanical rigidity while maintaining good optical quality. In the previous FDCD/FL-CE system, a section of the capillary's polyimide coating was removed under a gentle flame. This detection region was held between two U-shaped pieces of polycarbonate which formed a clamp. Approximately 1 cm of the capillary containing the optical region was positioned between the two arms of the clamp. Each arm contained a narrow groove to help align the capillary

and hold it in place. Although this clamp allowed for convenient installation of new capillaries, a more rigid mount was desirable. The requirements of compactness and maneuverability, essential in any on-column detector with tight focusing and low f-number collection optics made gluing the detector region to the edge of a small, thin plate a more favorable alternative.

In the new system a fast-fixing, hard epoxy (Devcon) is used to firmly attach the capillary to a 1" x 1" section of a standard 1/16" thick glass microscope slide. The glass slide contains a narrow notch at the position of the optical region (cell) to reduce light scatter and to facilitate cleaning of the cylindrical cell. The distance between points of attachment has been reduced to about 1 mm. A diagram of the new mounting arrangement (not drawn to scale) is given in Figure 14. In this view, the laser beam travels into the plane of the paper (along the z-axis). The side of the plate opposite the notch is epoxied to a short 1/4" diameter polycarbonate rod such that the capillary makes an angle of 30 to 40 degrees with the y-axis when mounted. This is to minimize collection along the x-axis of much of the scattered laser light as described earlier (*71*). The capillary assembly is clamped to a magnetic base (Newport Research Corp., Fountain Valley, CA, Model MB-2) allowing maximum versatility in positioning of the capillary cell on the optical table. The polycarbonate rod can be rotated about the x-axis for fine adjustment to maintain the capillary axis at 90° to the incident beam. The long section of capillary between the high voltage (HV) isolation

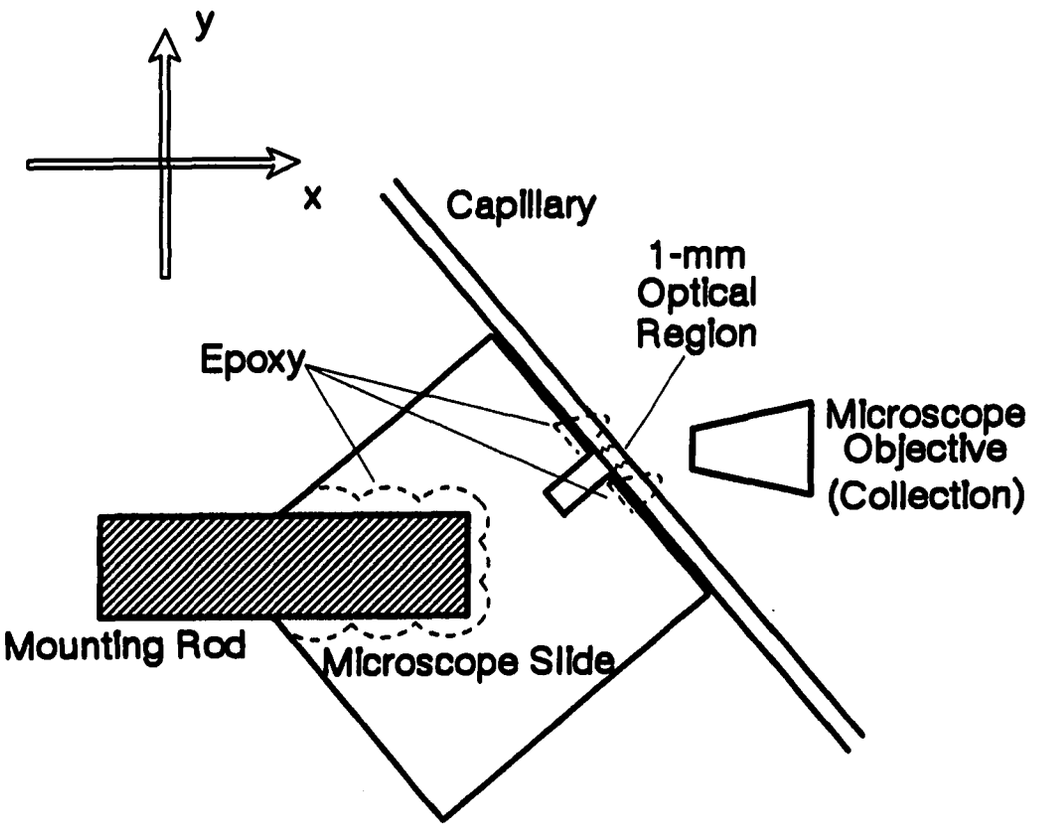

Figure 14. Capillary detection region and mounting arrangement

box and detector mount is taped to mounting posts at several positions to reduce the swaying that occurs when HV is turned on and off.

This mounting method has several advantages over the earlier one. It is more compact making it easier to position the capillary closer to the focusing lens and the collection optics. Any motion of the optical region has been significantly restricted by reducing the distance between points of attachment. The fragile optical region is better protected by the glass slide as evidenced by reduced frequency of breakage. Although the gluing method requires more time when a capillary is replaced, the procedure becomes routine with practice. The microscope slides are inexpensive and can be re-used after removing capillary and epoxy with heat.

Optical system

Many changes have been made in the optical system for on-column FDCD detection to improve detector performance. Figure 15 shows the detailed optical diagram as viewed from above the table with x, y, and z axes defined in the upper right-hand corner. The vertical y-axis points out of the plane of the paper. The beam path is horizontal (i.e., in the x-z plane) everywhere except between the beamsplitter (BS) and the first mirror (M_1) where a slight change in beam height is made. The 488-nm line of an argon ion laser (Control Laser Corp., Orlando, CA, Model 554A) operating under servo control at 1.2 W total power is separated from all other lines by an external 60° prism. Fifty percent of this line is reflected by a beamsplitter (Melles Griot, Irvine, CA)

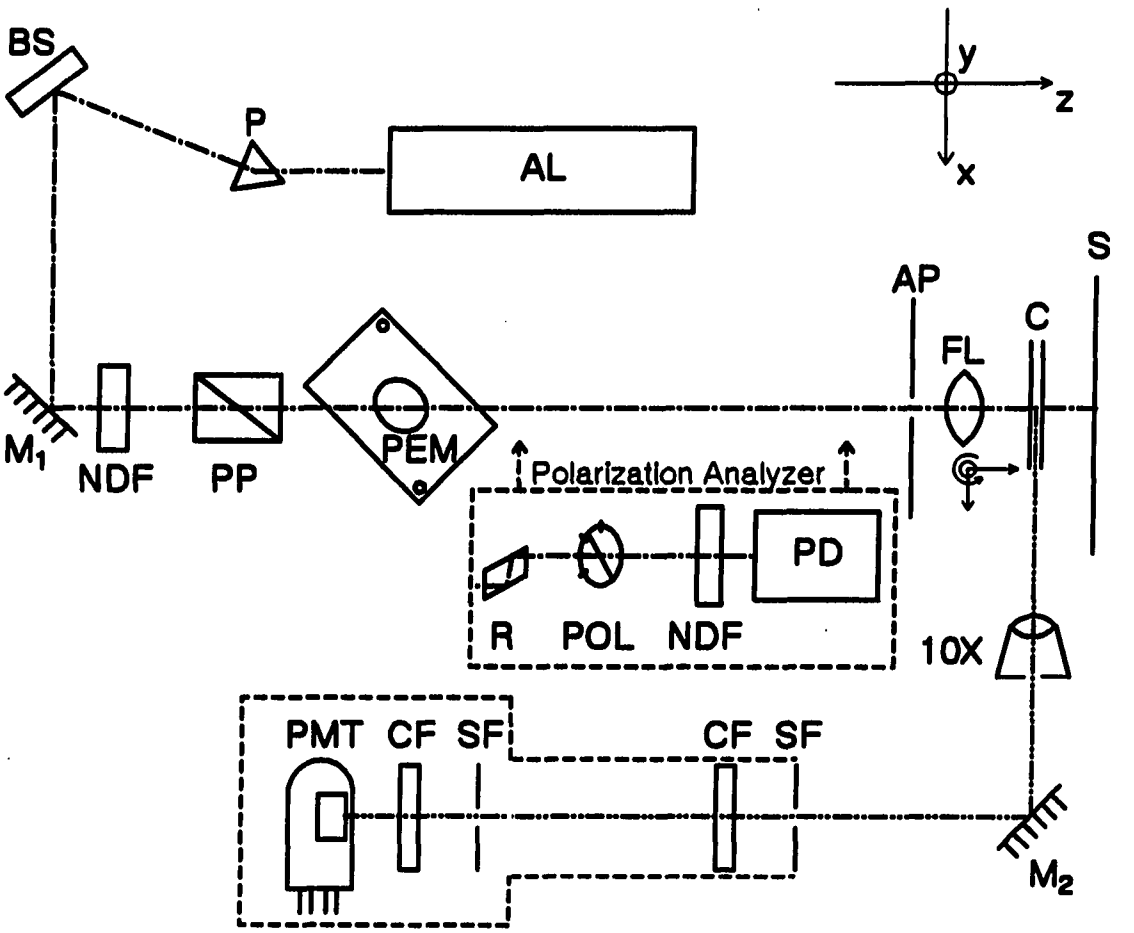

Figure 15. Detailed optical diagram for on-column FDCD/FL-CE viewed from above the optical table
(AL) Argon Ion Laser, (P) 60° Prism, (BS) Beamsplitter, (M_i) Mirrors, (NDF) Neutral Density Filters, (PP) Polarizing Prism, (PEM) Photoelastic Modulator, (R) Fresnel Rhomb, (LP) Linear Polarizer, (PD) Photodiode, (AP) Aperture, (FL) Focusing Lens, (C) Capillary Column, (S) Screen, (10X) Microscope Objective Lens, (SF) Spatial Filters, (CF) Color Filters, (PMT) Photomultiplier Tube.
-------- 488-nm incident beam.
-------- broadband fluorescence from sample in capillary.

and then by a mirror before attenuation by a neutral density filter (Melles Griot, Irvine, CA) of optical density 0.3 (50% transmitted). The resulting power at the polarizing prism is less than 100 mW. Although the laser output is vertically polarized (i.e., E-field along the y-axis), a calcite polarizing prism (Karl Lambrecht Corp., Chicago, IL, Model MGT-25-E8-90) set in a precision rotational stage (Aerotech Inc., Pittsburgh, PA, Model ATS-301R) is used to purify the polarization of this beam before modulation.

A photoelastic modulator (PEM), (Hinds, International, Inc., Hillsboro, OR, Model FS5) operating at 50 kHz replaces the Pockels cell for converting linearly polarized light into alternating left and right circularly polarized light (LCPL and RCPL). The large aperture and thinness of the PEM greatly facilitate optical alignment. The large aluminum dual-plate mirror-type mount used here fixes the modulator head so that the optical element is perpendicular to the propagation direction (z-axis) and so that the stress axis makes the prescribed 45° angle with the y-axis. The three-point mount allows for micrometer-driven adjustment of incident angle to optimize modulation efficiency while maintaining a fixed relationship between the modulator stress axis and the y-axis.

The polarization analyzer, comprised of Fresnel rhomb, linear polarizer, and photodiode, is used as described in Chapters II and III to monitor efficiency and balance of circular modulation. The analyzer is placed in the beam path during preliminary optimization and is retracted during FDCD measurements. Introduction of any optical element

oriented for non-normal incidence to divert a small portion of the beam alters the polarization of the reflected beam and precludes polarization analysis during the FDCD measurement.

A high quality fused silica lens (1-cm diameter, 1-cm focal length) (Oriel, Stratford, CT, Catalog No. 39301) focuses the laser beam into the capillary detection region. The lens is mounted on a high-precision 2-dimensional stage (Newport Research Corp., Fountain Valley, CA, Model 462-x-y) and can be rotated about the y-axis. A screen is placed behind the capillary cell to allow for visualization of the transmitted beam. Collection optics are identical to those described in Chapter III except that the second color filter is replaced (Schott Glass, No. OG515) to improve rejection of the scattered laser light.

Electronics

The photoelastic modulator is driven by a dedicated controller unit (Hinds International, Inc., Hillsboro, OR, PEM-80). The TTL-compatible square wave phase reference output at the modulator frequency (50 kHz) supplies the reference input for the lock-in amplifier (EG&G, Princeton Applied Research, Princeton, NJ, Model 5309 or 124A) and the external trigger input for an oscilloscope (Tektronix, Beaverton, OR, 7704A). A commercial current-sensitive preamplifier (EG&G, Princeton Applied Research, Princeton, NJ, Model 181) replaces the 10-kΩ passive resistor used previously for conversion of PMT current to voltage. This amplifier has two outputs of slightly different impedance. One output supplies signal to the lock-in amplifier/digital multimeter/chart recorder as described in Chapter III, while the other is sent to a

computer for recording of direct fluorescence signal. The lock-in amplifier is operated with band pass filtering centered at 50 kHz, the signal frequency, and with an output time constant of 300 ms. Data acquisition is performed at 40 Hz (20 Hz on either channel) by a 16-bit A/D converter (Data Translation, Marlboro, MA, DT2827) installed on an IBM PC/AT.

Reagents and samples

All solutions were prepared using deionized water (Millipore Corp., Bedford, MA, Milli-Q System). A 5×10^{-3} M sodium bicarbonate (Fisher Scientific, Fair Lawn, NJ, Certified Grade) solution of pH 9.5 was used as the electrophoretic running buffer throughout this work. Electrophoresis samples were also prepared in this buffer. The buffer pH was adjusted by addition of sodium hydroxide solution. The gradual change in pH that typically occurs for carbonate buffers upon exposure to air was negligible for this buffer concentration for up to 12 hours. Hence, the nitrogen purging was discontinued. The pH of the buffer was checked daily and adjusted as necessary.

Riboflavin standards were prepared by dissolving (-)-riboflavin (Aldrich Chemical, Milwaukee, WI, 98% pure) in the buffer described above. A 1×10^{-2} M stock solution of fluorescein (Molecular Probes, Eugene, OR, high purity acid form) was prepared by dissolving a weighed amount in NaOH and diluting to 100 mL with deionized water. Standard fluorescein samples were prepared by diluting μL quantities of stock solution with the electrophoresis buffer.

Fluorescein isothiocyanate (FITC) isomer I, also known as fluorescein-5-isothiocyanate, was obtained from Molecular Probes (Eugene, OR) and was used without further purification. L-amino acids were obtained from Pierce (Rockford, IL), Alltech (Deerfield, IL), and Sigma (St. Louis, MO). All D-amino acids were from Chemical Dynamics (South Plainfield, NJ). Acetone and pyridine (Fisher, Fair Lawn, NJ) were used as received. FTC-amino acids were prepared using modifications of a published procedure (*81*). Details of the reaction conditions are discussed in a later section. In all cases, excess amino acid was added to the reaction mixture to reduce the background fluorescence from the reagent. Reactions were carried out in the electrophoresis buffer, 5 mM sodium bicarbonate at pH 9.5. The mixtures were not acidified to precipitate and isolate the FTC-amino acids, but were simply stored as the reacting mixture. Electrophoresis samples were taken directly from the reaction mixture. All fluorophore solutions were stored in the dark at 4 °C.

Results and Discussion

The results of this work are divided into two parts. The first section deals with the refinements made in the on-column FDCD detector increasing its utility and reliability. Performance is tested with two fluorophores, optically active riboflavin and optically inactive fluorescein, as done in Chapter III. The second section concerns the analysis of FTC-amino acids by CE using the refined FDCD/FL detection system.

Optimization of instrumentation

Modulator The limitations of the first FDCD/FL-CE system were attributed in part to the Pockels cell modulator. A photoelastic modulator (PEM) replaces the Pockels cell in the present system and is found to be superior in several respects. Because the optical element of the PEM is only 1/16 inch thick and has a clear aperture diameter of 0.70 inch, it is much simpler to align than the Pockels cell. The large angular acceptance (40°) of the PEM permits its use with small, collimated beams of light from a laser source as well as with larger diverging (or converging) beams. By design, the PEM has maximum retardation efficiency at the center of the optical element. This efficiency decreases uniformly in all directions from this point. Thus, it is most desirable to have the incident beam centered on the optical element.

In contrast to the Pockels cell which required relatively large driving voltages ($V_{avg} \simeq 150$ V, $\Delta V \simeq 120$ V), the PEM is driven by a 5-V signal from the controller. Hence, the electrical noise generated by the modulation system is reduced considerably. The desired retardation is selected by setting the peak-to-peak retardation amplitude on the front of the PEM controller unit. The value displayed corresponds to the wavelength (in nm) where ±½-wave retardation occurs. The conversion of linearly polarized light into left and right circularly polarized light requires ±¼-wave retardation, Hence, a peak-to-peak retardation setting of 244 nm is required to obtain circular modulation at 488 nm.

The efficiency of modulation is monitored with the polarization analyzer (see Figure 15). Here, the Fresnel rhomb introduces 90° (or ¼-wave) retardation and converts the two circular polarizations into orthogonal linear polarizations. The intensity of light transmitted by a linear polarizer is measured at the photodiode and displayed on an oscilloscope. The polarizer transmission axis is at an angle θ with respect to vertical. In this way the modulation efficiency (percent modulation depth) for each circular polarization and the balance in intensity of left and right circular polarizations can be visualized as they alternate at the PEM frequency (50 kHz). Figure 16 shows the oscilloscope trace from the polarization analyzer during PEM operation. The linear polarizer axis is fixed at 0° (for vertical transmission) in each of the four cases presented. Here, one observes intensity modulation of one particular circular polarization. The other polarization can be observed when θ is set to 90°. Figure 16 shows how modulation depth changes with increasing peak-to-peak retardation amplitude. We observe that ¼-wave modulation efficiency increases as retardation amplitude increases. In the present system, optimum sinusoidal modulation is obtained for a retardation setting of about 222 nm. Above the 222-nm setting, the shape of the modulation waveform becomes distorted. Notice how the sinusoidal waveform in b begins to flatten out in c. It eventually exhibits inverted peaks in d. This is typical behavior of all photoelastic modulators. It is important to adjust retardation amplitude for optimum performance with any given light source.

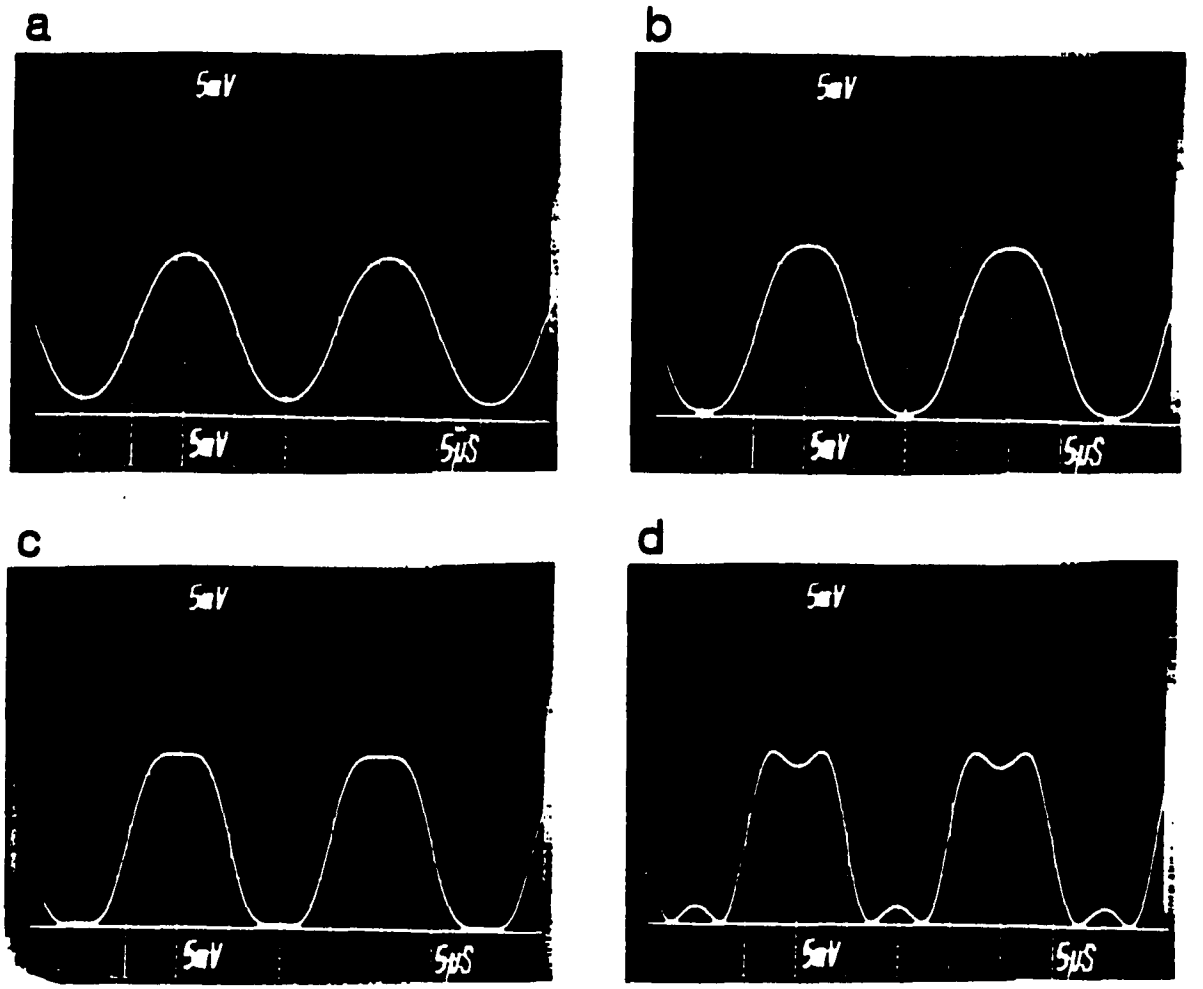

Figure 16. Polarization analyzer signal showing changes in modulation depth as PEM retardation amplitude is increased
Linear polarizer axis set vertical (θ = 0°) in a-d. PEM peak-to-peak retardation amplitude (λ of ±½-wave retardation):
(a) 150 nm, (b) 200 nm, (c) 244 nm, (d) 375 nm.
See text for details.

In the FDCD experiment, the intensities of left and right circularly polarized light must be well balanced. We can observe modulation balance with the same polarization analyzer. After the retardation amplitude has been set for maximum modulation efficiency, the PEM position is fine-tuned until the modulation waveforms for $\theta = 0°$ and $\theta = 90°$ have identical maximum and minimum values indicating $I_{0,L} = I_{0,R}$. The difference between maximum and minimum values should be as large as possible with the minimum values at or very near zero showing that modulation depth is maintained. To assure that any unmodulated fraction of light will also be balanced, we check the polarization analyzer signals for $\theta = 45°$ and $\theta = 135°$. Both should exhibit dc response centered at the average value of the waveform obtained when $\theta = 0°$ or $\theta = 90°$. These 45° and 135° signals may have a minor 100 kHz ripple but care should be taken during the alignment process to eliminate any 50 kHz signal at these polarizer settings.

An example of polarization analyzer signals under optimized conditions for modulation efficiency and balance is given in Figure 17. In contrast to the Pockels cell, modulation efficiencies in excess of 98% are routinely obtained with minimal alignment effort using the PEM. We have found that optimum performance and tunability are obtained when the calcite polarizing prism is placed before the PEM to further purify the linear polarization. This is reasonable because the primary limitation of PEM operation is the input polarization purity (*2*). Fine adjustment of the polarizing prism axis greatly facilitates balancing of modulation.

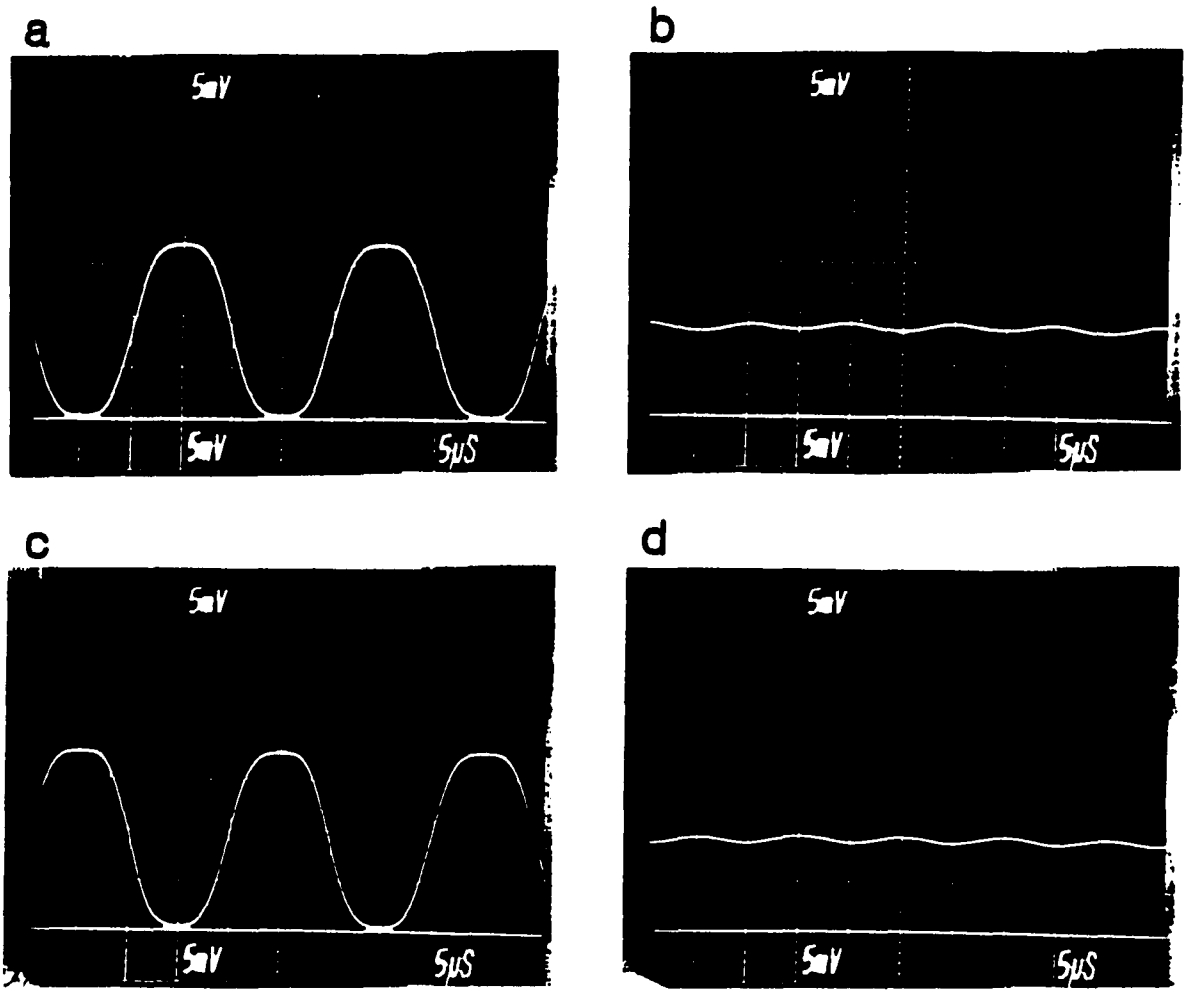

Figure 17. Polarization analyzer signal showing optimized modulation efficiency and balance
(a) $\theta = 0°$, (b) $\theta = 45°$, (c) $\theta = 90°$, (d) $\theta = 135°$.
See text for details.

A 5× telescope was used in early experiments to expand the 1-mm-diameter laser beam to fill more of the PEM clear aperture and decrease the effect of any local imperfections in the crystal. However, no improvements in discrimination of artifacts were observed with such an arrangement. For the studies reported here, the collimated laser beam passes through the center of the PEM without prior expansion.

Optical train After the installation of the PEM, several observations indicated that problems with other optical components and general optical alignment were still limiting our ability to discriminate against non-CD artifacts. The discrimination ratio, r (defined in Chapter III, page 52), was used to assess discrimination in electropherograms of optically active riboflavin and optically inactive fluorescein. Although good modulation balance and efficiency were routinely detected after the PEM, acceptable discrimination in FDCD signals ($|r| < 0.1$) could not be obtained routinely. The problems in obtaining good discrimination were shown by the uncontrollable appearance of FDCD artifact signals for fluorescein. Inconsistency in discrimination was seen even though the procedure for aligning optical components (i.e., monitoring transmitted beam quality and image of detection region at the PMT) and for setting lock-in amplifier (LIA) phase to lock onto riboflavin signal remained unchanged. Sometimes the method produced good discrimination, but often times it did not. Even when good discrimination was obtained, it slowly degraded over time and could not be maintained from one day to the next.

Ideally, one would see the desired FDCD response for riboflavin (R) and negligible response for fluorescein (F). Frequently, we observed FDCD signals for each compound which were proportional to their respective FL signals regardless of LIA phase setting (i.e., $(FDCD/FL)_F \propto (FDCD/FL)_R$). This indicated imbalance in the incident intensity within the capillary on the two half cycles of modulation. The magnitude of the imbalance often overwhelmed the true FDCD signal. Intensity modulation of this type could result from unbalanced PEM operation which is too small to be detected by the polarization analyzer. Intensity modulation may also result from preferential reflection loss of one circular component at an off-axis (non-perpendicular) optical surface. The lens and capillary had been aligned for perpendicular incidence as nearly as could be determined visually without micropositioners and more sophisticated alignment tools. However, these alignment efforts alone were not sufficient to remove all FDCD artifacts.

Occasionally the maximum FDCD signal for riboflavin was obtained at one LIA phase setting, while fluorescein produced an FDCD artifact that gave maximum signal for a different phase setting. This indicated that a relative phase shift between left and right components was occurring upon passage through the lens and capillary. It was difficult to determine whether the lens or capillary was more responsible for this because the required 1-cm spacing between these components made it impossible to monitor the polarization state between them. It is likely that both lens and capillary contributed to this birefringence. Both

the lens and capillary should be amorphous since they are made of fused silica (or glass), but they could contain small regions of imperfection or strain which produce circular birefringence. This would severely affect the polarization state by imparting a delay (or phase shift) between the left and right circular components. The resulting modulation would be between different elliptical polarizations, and the light inside the capillary would exhibit intensity modulation at 50 kHz. Under such conditions, the LIA phase setting for maximum riboflavin FDCD could differ from that phase setting which locks onto the incident intensity modulation causing maximum artifact signals, as was sometimes observed.

The difficulties in achieving FDCD reproducibility emphasized the need for further improvements in the optical system. Mounting the focusing lens on a heavy, two-dimensional stage with high translation precision permitted a more careful study of alignment effects and resulted in important observations. A very small translation (<1μm) of the focusing lens, which had no visible effect on the transmitted beam profile or in the fluorescent image at the PMT, produced drastic changes in the FDCD artifact signals. Not only did lens translation cause changes in artifact signal magnitude, but frequently it resulted in sign reversal as well. Similar effects were observed if the lens remained fixed and the capillary cell was moved. Furthermore, controlled movement of the lens during constant flow of riboflavin showed that maximum FL and FDCD signals did not necessarily occur for the same alignment conditions. Thus, it is apparent that precise

alignment of the focusing lens and capillary cell are critical in optimization of FDCD and elimination of artifacts. Previously, positions of optical components were adjusted to maximize fluorescence signal while retaining good transmitted beam quality and a crisp image of the capillary walls and sample fluorescence before the PMT. It is now obvious that more accuracy in alignment procedure is necessary.

The collection and detection optics (microscope objective, mirror, filters, PMT) can also contribute to artifacts if modulation is unbalanced and a significant amount of the scattered laser light (which is polarized) is collected. Ideally, the PMT used for any transmission CD measurement should have a flat window surface to prevent artifacts (*2*). However, because we measure fluorescence emission from a non-rigid (i.e., freely rotating) sample on a microsecond time scale (50 kHz), the polarization at the detector should be completely randomized. Hence, in principle the end-on type PMT requirement can be ignored for FDCD. The side-on PMT used in these studies has a cylindrical window. Experiments in which the image position and angle of incidence at the PMT were varied indicated qualitatively that FDCD signals were only sensitive to alignment of collection optics when discrimination was poor. Under conditions of good artifact discrimination, very little change was seen in FDCD signals as collection optics were adjusted. In general, the artifacts we observed were much less sensitive to changes in alignment of the collection optics as compared to the incident optics. Once it became apparent that the alignment of the lens and capillary was the most critical factor in

artifact discrimination, several steps were taken to reduce imperfections and stray birefringence in these components and to allow more precise control of alignment.

Several of the glass lenses used previously in the FDCD system displayed orange-red fluorescence when placed in the 488-nm beam path. This fluorescence, which likely added background noise in FDCD and FL measurements, was eliminated when a high quality fused silica lens was used. Mounting the lens with rotational adjustment capability about the y-axis (see Figure 15) improved alignment accuracy.

The cylindrical capillary detection cell must also be of good optical quality to prevent FDCD artifacts. The heat used to remove the polyimide coating from the observation region on the capillary could bend or otherwise distort the capillary. The tendency to produce such distortions increases if too much heat is applied or if unbalanced forces act on this region during the heating process. Taping the capillary to the glass slide mount before removing the coating increases the likelihood of obtaining a good quality detection cell. Holding the capillary by the cell mount during heating allows more controlled heating and eliminates the need to handle the fragile capillary directly. The free-hanging ends of the capillary exert no force on the heated region since the capillary is firmly taped to the glass slide on both sides of the optical region. The glass slide protects much of the capillary from direct heat and allows for selective burning of the coating from only the 1-mm segment at the notch. With such a small

section of coating removed, the capillary retains much of its resilience.

After the coating is removed and the region is cleaned with a tissue soaked in methanol, the cell is viewed under a microscope to verify that no distortion of cell walls has occurred. Once the symmetry of the optical cell is confirmed, epoxy is applied to either side of the notch to permanently attach the optical region to the glass slide. This procedure is found to be the most efficient method which routinely produces good quality on-column detection cells suitable for FDCD. The initial rinsing and filling of the capillaries is often delayed until after a satisfactory detection region has been obtained and is securely mounted.

Electronics Several necessary improvements have been made in the electronics associated with the FDCD/FL system. The decrease in electrical noise generated by the PEM as compared to the Pockels cell has already been discussed. In the previous FDCD/FL-CE system, a passive resistor circuit converted the PMT current to voltage and amplified the signal. Although such a circuit works adequately in some systems, it was particularly problematic in the FDCD/FL system where the PMT signal is simultaneously sent to two independent channels for recovery of dc (FL) and ac (FDCD) signals. The simple resistor circuit alone could not prevent electrical feedback between the two channels. Sharp signals (spikes) corresponding to a change in the dc fluorescence signal level were occasionally observed on the LIA output and interfered

with FDCD measurements. Using a high pass RC circuit filter on the LIA input reduced the magnitude of these spikes but did not eliminate them.

A commercially available current preamplifier solved these problems very conveniently. The amplifier output can be divided and sent to both ac and dc channels without any feedback interference. The amplifier used in this work (EG&G, Princeton Applied Research, Princeton, NJ, Model 181) has a second isolated output which is useful when two dual-channel recording systems (chart recorder and computer) are employed simultaneously. Selectable amplification range and an overload indicator light add to the convenience of this amplifier. The electrical connection between the PMT and the amplifier is made with a short cable (approximately 30 cm) to reduce capacitance and antenna effects.

Two newer model lock-in amplifiers (EG&G, Princeton Applied Research, Princeton, NJ) were tested in the present FDCD system. Both the 124A, which is strictly an analog instrument, and the 5209, which contains a microprocessor, give satisfactory results. The Signal Monitor output of the LIA provides the filtered and amplified input signal before demodulation occurs. This signal provides the most sensitive and direct observation of amplitude modulation on the LIA input. The modulated signal is easily displayed on an oscilloscope and is an invaluable tool during optimization of the FDCD detector. It provides the best method for monitoring non-CD artifacts which result from residual amplitude modulation. By observing this signal, we see directly whether any modulated fluorescence signal is present. When

riboflavin flows through the detection region, we expect to see a 50 kHz sine wave signal. Alternatively, when a CD-inactive fluorophore such as fluorescein is probed, the modulated signal should disappear. Any 50 kHz ripple seen for fluorescein indicates that an artifact condition exists. The use of this Signal Monitor output is described more fully in the following section.

Procedure The changes made in the optics and electronics permitted the development of a more effective procedure for optimization of FDCD and elimination of artifacts. During preliminary alignment, careful placement of optics is required to insure that the beam path remains horizontal (i.e., in the x-z plane as defined in Figure 15) beyond M_1 and that each optical surface lies perpendicular to the propagation direction. Modulation balance and efficiency are optimized as described above. Before the focusing lens is inserted, the mounted capillary is set in place. When the capillary cell is appropriately centered in the collimated beam, a symmetrical beam image, bisected by the capillary, is observed on the screen. Proper placement of the focusing lens is achieved when the beam passes through the center of the previously positioned capillary cell. The transmitted beam, now larger and diverging, must be centered about the original beam position on the screen. The aperture that is before the lens rejects extraneous room light and acts as a visualization screen to display the portion of incident light which is reflected at each lens surface. These reflected spots are used as alignment aids. When the lens is properly aligned, the reflected circular spots overlap and propagate symmetrically back

along the incident beam path. The distance between the lens and capillary is optimized for maximum fluorescence signal and minimum distortion of the transmitted beam.

The collection optics are mounted for 90° collection at the same height as the incident beam. The capillary cell holder is rotated about the x-axis to obtain a vertical image of the capillary cell in front of the PMT. This insures that normal incidence occurs at the capillary. Color filters and spatial filters are then inserted to reject the blue light that is scattered from the capillary walls. The yellow-green fluorescence spot from samples within the capillary falls on the center of the PMT cathode.

The final step in FDCD alignment is fine tuning the lens position to optically null artifact signals. To accomplish this an optically inactive fluorophore is introduced and the output of the LIA Signal Monitor is displayed on an oscilloscope. If the preliminary alignment and preparation of a suitable capillary have been done carefully, complete removal of any artifact can be accomplished by very slight adjustment of the lens alone. During this nulling process, significant phase changes in the 50 kHz artifact signal can be observed in the shifting of the displayed waveform. In fact, large changes in the modulated signal can be produced by lens movement so minor that dc fluorescence changes very little and no change is discernible in the transmitted and reflected beam shapes or positions. This reconfirms the extreme sensitivity of artifact signals on the incident alignment conditions and establishes the need to optically null artifacts while

monitoring both ac and dc signals electronically. Clearly, the typical alignment method used for direct fluorescence detection alone in CE is not sufficient to obtain satisfactory FDCD measurements. At this point, collection optics can be adjusted to maximize the total FL signal from the PMT. Any part of the preliminary alignment procedure can be repeated as long as the removal of the non-CD artifacts is verified each time any changes are made.

Once optical artifacts have been removed, an optically active fluorophore is introduced to enable optimization of LIA phase for maximum FDCD signal output. For LIAs with manual phase selection, the phase is adjusted more accurately for zero output and then flipped by 90° to measure FDCD. In LIAs with automatic phase setting capabilities, the appropriate phase is selected by the LIA to maximize the FDCD output.

The optimization procedures outlined above have resulted in a much improved FDCD/FL detector for CE. Good discrimination levels ($|r| < 0.1$) for riboflavin have been repeatedly obtained using these methods. Figure 18 shows a typical example of the FDCD/FL-CE results for a sample containing riboflavin and fluorescein. The migration time (t_m) for each peak can be determined from the x-axis. The direct fluorescence signals for the two components are nearly equal as shown in Figure 18a. Figure 18b gives the demodulated LIA output (FDCD signal) obtained for the same injection as in Figure 18a. The LIA phase in 18b (285°) is set for optimum FDCD signals. This condition is identified as the "signal phase." The discrimination ratio, r, for this measurement

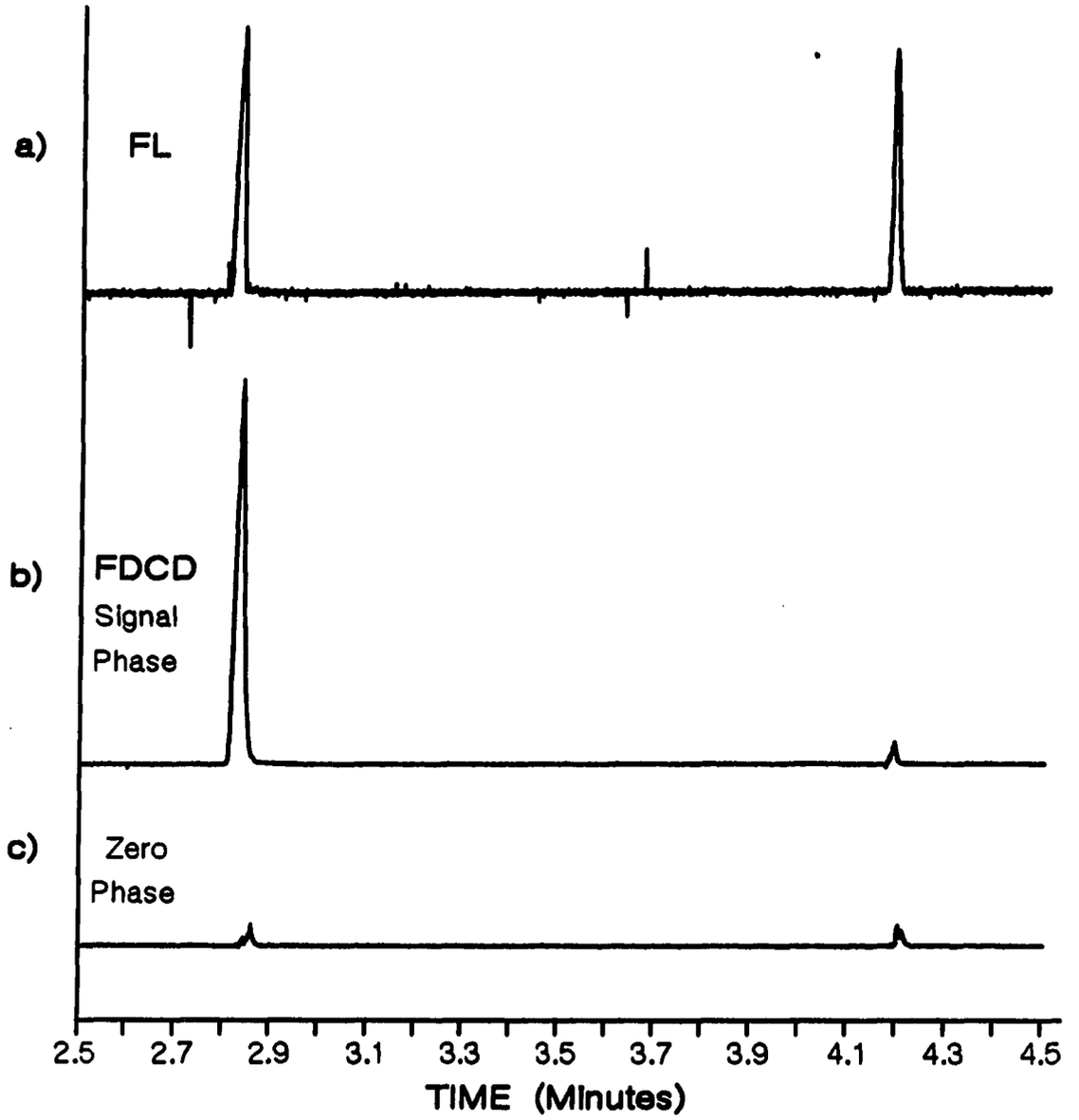

Figure 18. Optimized FDCD/FL-CE signals for separation of riboflavin (t_m = 2.85 min) and fluorescein (t_m = 4.2 min)
(a) Direct fluorescence. (b) Optimized FDCD signal for LIA on signal phase. (c) FDCD signal on LIA zero phase. FDCD scale is constant for b and c. See text for details.

is +0.06 and demonstrates high selectivity for the optically active component, riboflavin. In Figure 18c the LIA phase (195°) has been shifted by 90° and is identified as the "zero phase." This demodulated output was obtained for a second injection of the same sample mixture. The FL trace for this second run, though not shown here, is identical to that in Figure 18a. Figure 18c indicates that the LIA registers a small signal for each component at the zero phase. Although these signals resemble artifact peaks, closer examination and additional experiments confirm that they lie within the noise associated with the measurement. In each case, this noise is proportional to the corresponding dc fluorescence signal. FDCD response obtained for fluorescein at the signal phase also lies within the noise. Thus, the once prominent optical artifacts resulting from birefringence in incident optics and residual amplitude modulation have been effectively suppressed by the methods described here.

The optimized FDCD system also achieves greater signal-to-noise (S/N) than the previous version did. We have defined a stability measurement for the FDCD/FL-CE system as $\frac{1}{2}(I_F/N)$. Here, I_F represents the total dc fluorescence signal going to the LIA (in mV), and N is the peak-to-peak noise on the demodulated LIA output. The measurement is based on noise recorded for a minimum of 30 s and the LIA sensitivity scale is taken into account. Previously, a LIA output time constant (τ) of 1 s was used. However, because migrating zones in CE can pass through the detector region very quickly (on the order of a few seconds), a shorter time constant is preferable to prevent distortion of

the signal. Comparing typical FDCD-CE peaks for different values of τ showed that notable attenuation occurs for τ = 1 s, but little change in peak height was observed for 300 ms $\leq \tau \leq$ 10 ms. A time constant of 300 ms is found to provide the most favorable noise reduction with adequate response time. Stability measurements exceeding 5000 (τ = 300 ms) are routinely obtained with the optimized FDCD/FL-CE system demonstrating improvement over earlier results.

Another type of stability is monitored by the drift in artifact discrimination levels. Although the FDCD refinements described in this chapter have reduced drifting, efforts to eliminate it have not yet been successful. Figure 19 presents an example of the drift in discrimination observed over time. Excellent discrimination is demonstrated in 19a (r = -0.04), which was recorded immediately after nulling the 50 kHz artifact and setting phase. As second injection of the same sample 2.6 hours later produced the signals shown in Figure 19b. It is obvious that a measurable artifact signal (r = 0.68) appeared during the elapsed time even though optical components were untouched. Excellent discrimination was reestablished by repeating the lens optimization procedure nulling the fluorescein artifact. The optimum LIA phase setting was not altered by the nulling process. A third injection of riboflavin and fluorescein, which shows the regained discrimination (r = 0.08) is displayed in Figure 19c.

The LIA time constant varies from 300 ms to 100 ms to 30 ms for Figures 19a, 19b, and 19c, respectively. Measurement of r becomes difficult when discrimination is very good because the FDCD artifact

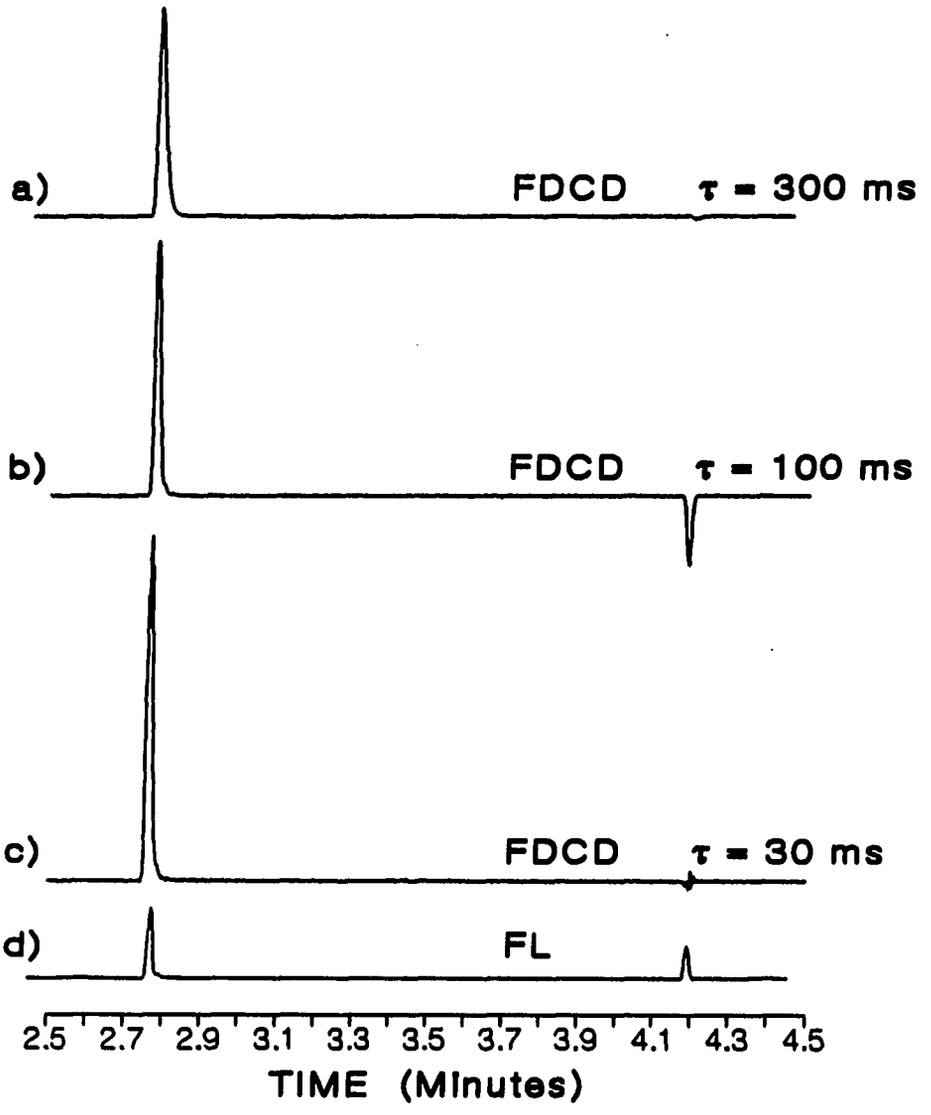

Figure 19. FDCD and FL signals for separation of riboflavin (t_m = 2.8 min) and fluorescein (t_m = 4.2 min) showing ability to optically null artifacts after drift in discrimination (a) Initial FDCD signal obtained just after optimization. (b) FDCD signal for the same sample after 2.6 hours. (c) FDCD signal for same sample after 3 hours and reoptimization procedure. (d) Fluorescence signal obtained during a, representative of all three injections, a-c. FDCD scale is constant in a-c.

peak for the inactive component is reduced to noise fluctuations on the LIA baseline. This can be seen most clearly by the baseline crossings seen for τ = 30 ms in Figure 19c. The artifact in Figure 19b causes a slight reduction in riboflavin FDCD signal, but does not severely limit detectability by FDCD.

It is now possible to achieve good discrimination repeatedly using the systematic approach outlined here. Drifting is still observed, but the nulling procedure described requires only 10 minutes and repeatedly regains optimal discrimination of artifacts. The instrument has, on occasion, demonstrated excellent discrimination from one day to the next with no operator adjustment required. Hence, long-term stability has also been improved in the optimized FDCD/FL-CE system.

In the past we noted photodecomposition of riboflavin samples and suggested that samples be prepared daily. Since optimization and comparison of FDCD system performance are based on riboflavin FDCD measurements, the stability of riboflavin in solution is important. Figure 20 presents the variation in standard CD spectra (obtained on an AVIV Associates 62DS CD Spectrometer) for a single riboflavin sample taken immediately after dissolution and after 0.4 and 3.2 hours. These spectra indicate that CD signal decreases significantly over a period of a few hours, whereas the decomposition product was not evident in the FL electropherogram until much later. The decreasing CD signal may be the result of racemization or decomposition. Whatever the cause, it is now apparent that quantitative comparisons of riboflavin FDCD require more frequent sample preparation.

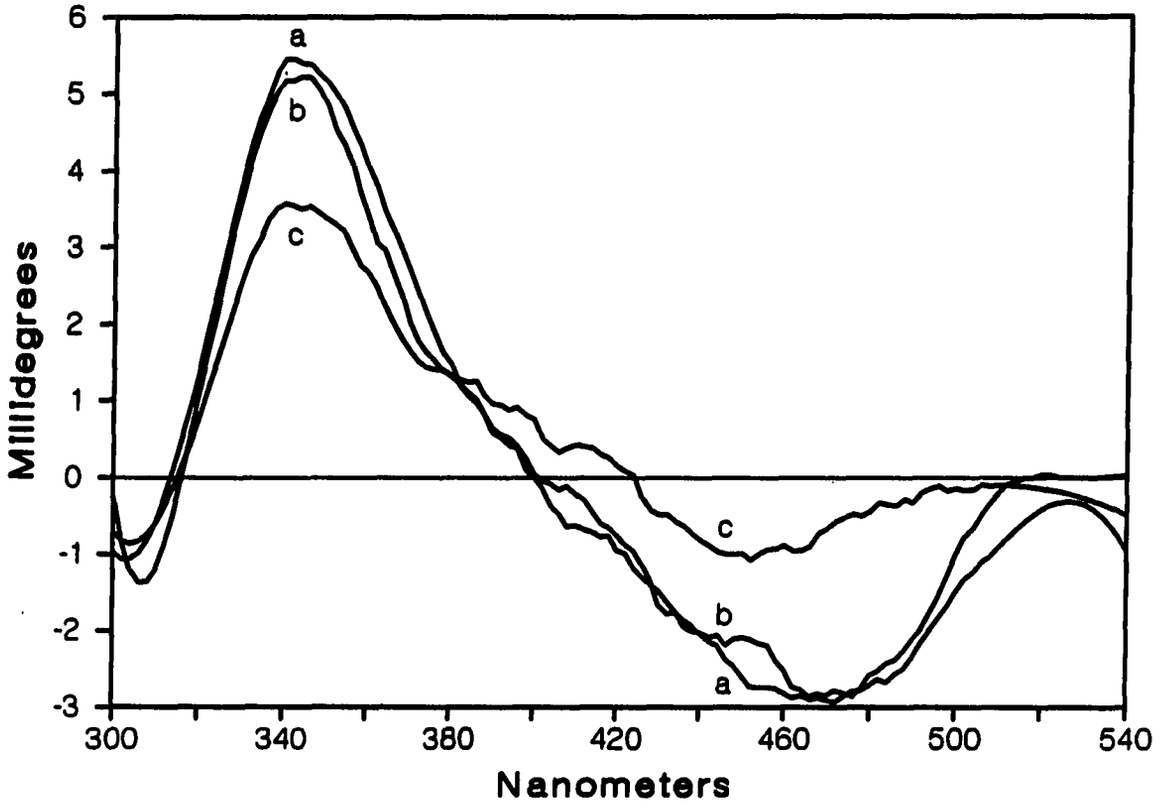

Figure 20. CD spectra of riboflavin in 5×10^{-3} M $NaHCO_3$ at pH 9.5
(a) Freshly prepared. (b) 26 minutes after dissolution.
(c) 3 hours 10 minutes after dissolution.

The difficulties in FDCD/FL-CE are now more clearly understood, and advances have been made in the design and operation of the instrument. Further improvements may be possible as more stable micropositioners become available and as pointing stability of laser sources is improved. The laser used for these studies did not display optimal mode structure, and this may be partially responsible for the difficulties encountered. Ideally, the laser source would have TEM_{00} mode for this technique. In addition, annealing of lens and capillary at high temperatures to remove residual birefringence may simplify the optimization procedure and may be necessary to achieve the ultimate in FDCD performance.

Application of FDCD/FL-CE to derivatized amino acids

Derivatization with FITC With the FDCD/FL-CE instrument operating more reliably, it became feasible to pursue FDCD studies of derivatized amino acids. FTC-derivatives of the 20 common protein amino acids (L-conformations only) were prepared with FITC-I using Kawauchi's procedure (*87*) as a guide. The reactions were carried out in 2×10^{-3} M sodium bicarbonate at pH 9.45 and contained a 10-fold molar excess of amino acid relative to the FITC reagent. Initially, each reaction mixture was analyzed by rapid CE with direct fluorescence detection. This preliminary screening (data not shown) confirmed that each of the natural amino acids formed at least one distinguishable FTC-derivative. Arginine (Arg) and lysine (Lys), which contain primary amino groups in their R group side chains, can be doubly derivatized. Both Arg and Lys produced two FTC-derivative peaks in the electro-

phoretic separations. Cysteine (Cys), which commonly exists in multiple forms in solution, produced one major fluorescent component and three minor ones upon derivatization with FITC. The minor peaks may result from reaction of FITC with the sulfhydryl groups (*73*). All other amino acids produced a single FTC-amino acid component.

Reaction rates and extent of derivatization vary for the different amino acids and for different reaction conditions. FTC-amino acid peaks can be detected a few minutes after mixing, but the reaction may not reach equilibrium/completion for several hours. Gently heating the reaction mixtures to 30 °C using a temperature-controlled water bath and sonicating for a period of one hour in an ultrasonic bath at 42 °C were explored as methods to speed the reaction, but neither improved the rate significantly. More rigorous heating methods were avoided to reduce the chances of racemization. We typically placed all reaction mixtures on a wrist-action shaker at room temperature for one to two hours after the initial mixing. The mixtures were not treated with acid at any time to halt the derivatization process or to precipitate the FTC-amino acid. All electrophoresis samples were taken directly from the reaction mixtures. Glutamic acid (Glu) and aspartc acid (Asp), which contain a second acid functionality, show the slowest reaction rates for derivatization, as is commonly observed (*80*, *84*), but still provide measurable FTC-derivatives within convenient reaction times.

Several peaks are present in the fluorescence electropherogram of the reagent blank, a solution containing all reagents except the amino acid. These background components also show up in each sample and are

attributed to unreacted FITC reagent, impurities in the FITC, and decomposition products of FITC. Occasionally minor peaks, which are not present in the blank, can be seen in the derivatized amino acid samples. These peaks likely represent FTC derivatives of impurities present in the original amino acid standards. When the FITC reagent is dissolved in acetone with a trace amount of pyridine before its addition to the amino acid standards and blank (as directed in reference *87*), the derivatized blank contains one major component (likely unreacted FITC). The amino acid derivatives prepared in this way also contain this component, but its fluorescence peak magnitude is reduced. For samples derivatized in this manner, the individual FTC-amino acid peaks dominate over the minor unidentified impurity peaks.

The results are somewhat different when the FITC is dissolved in NaOH and diluted with buffer before adding the amino acid. When this method is employed, a different component dominates the blank electropherogram and gives the most prominent peak in all the amino acid samples as well. Apparently, dissolution in strong base promotes the decomposition of the FITC reagent. This new peak may result from conversion of FITC to amino fluorescein *(87)* or fluorescein. Although the FTC-amino acids are still formed by this method and can be easily identified in the fluorescence electropherograms (see below) the yield for these desired derivatives decreases.

Others have reported multiple fluorescent products in the background for derivatizations with FITC (*49*, *86*). Signals from background components are a common problem with highly fluorescent

reagents such as FITC. Fortunately, these blank reaction products give reproducible electrophoresis behavior and are easily separated from the FTC-amino acids of interest. Some of the impurity peaks can be reduced by increasing the mole ratio of amino acid to FITC. In the experiments discussed below, the molar quantity of amino acid was increased to 50 or 100 times the FITC quantity. The stability of FTC-amino acid derivatives in solution was evaluated by comparison of fluorescence electropherograms for old and new sample mixtures. Samples that were kept at 4 °C for up to one month produced electropherograms similar to freshly prepared samples, and some FTC-amino acid derivatives were observed in solutions over two months old. However, the fluorescent impurities multiply with sample age and are more prominent in samples kept at room temperature.

Electrophoretic separations with FL and FDCD detection The fluorescence electropherograms for five selected FTC-amino acid derivatization mixtures and a blank are shown in Figure 21. From top to bottom these correspond to reaction of FITC-I with (a) blank, (b) glycine (Gly), (c) L-alanine (Ala), (d) L-phenylalanine (Phe), (e) L-serine (Ser), (f) L-tryptophan (Trp), and (g) a second injection of the FTC-glycine preparation. These samples were run on the same day they were prepared and are displayed in the order the data were obtained. Reagent concentrations in each mixture are approximately 1.4×10^{-3} M amino acid and 2.5×10^{-5} M FITC. These particular samples were prepared using FITC that had been dissolved in NaOH. Injection volume is estimated to be 2 nL. Hence, the maximum injected quantity

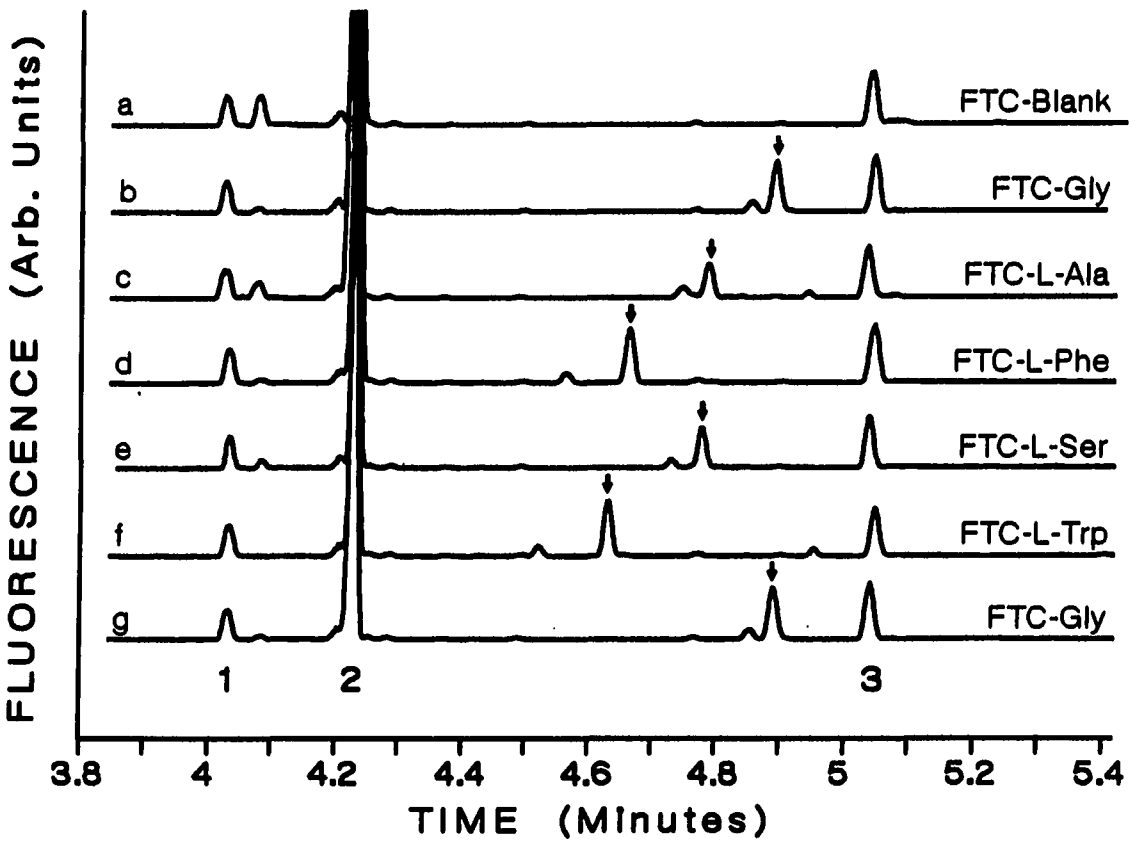

Figure 21. Fluorescence electropherograms for a set of FTC-amino acid derivatives and a blank reaction mixture
Fluorescence scale is constant for all 7 runs. Separation is performed at 28 kV on a 50-μm x 70-cm capillary. Injections are by electromigration for 1 s at 28 kV.

possible for each FTC-amino acid is calculated to be approximately 50 fmol. This assumes 100% conversion of FITC, the limiting reagent, to the desired product. This estimated value represents an upper limit for the amount injected because FITC obviously reacts to form more than one product and thereby reduces the concentration of FTC-amino acid in these mixtures.

The positions labeled **1**, **2**, and **3** above the time axis indicate the migration times for components that are observed in every sample prepared by this method. These three peaks are easily identified in each of the runs. Peak **2** (4.25 min.) is the largest peak in each sample and is attributed to the decomposition of FITC. Component **3**, though not identified, gives a relatively constant signal in all samples. The largest peak between peaks **2** and **3** corresponds to the FTC-amino acid present in each sample and is designated by an arrow in each electropherogram. The fluorescence signals for these five FTC-amino acids vary by less than a factor of two demonstrating reasonably uniform derivatization.

The FDCD signals obtained simultaneously with the FL signals of Figure 21 are displayed in Figure 22. Optical nulling of the non-CD artifact was done just prior to injection of the blank. The degree of discrimination achieved (r = -0.044) is shown in Figure 19a. The FDCD signal for (-)-riboflavin is the standard used for comparison in this study. The sign of an FDCD signal is determined by comparison with the riboflavin signal obtained under the same instrumental conditions. By this convention, FDCD signals going in the same direction as the

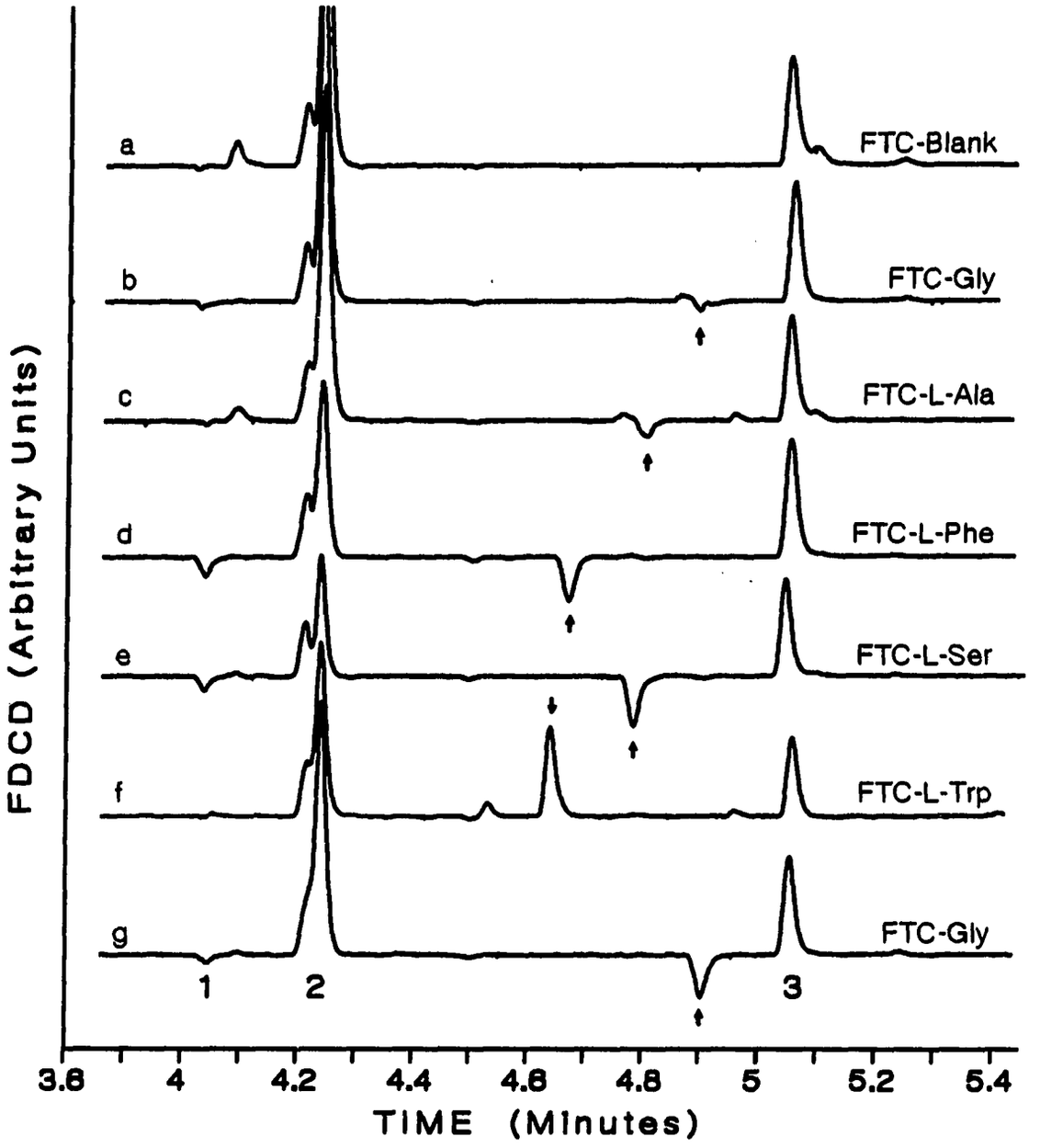

Figure 22. Fluorescence-detected circular dichroism (FDCD) signals obtained simultaneously with FL data in Figure 21 for a set of FTC-amino acid derivatives and a blank
FDCD scale is constant for all 7 runs. See Figure 21 and text for details.

riboflavin signal are classified as positive and those going in the opposite direction are negative. It should be noted that the y scales are not necessarily equivalent in Figures 18, 19, 21, and 22. Several interesting phenomena can be observed in the FDCD data for this set of amino acids derivatives. The measured FL and FDCD peak heights and the FDCD/FL ratios for these runs are tabulated in Table 2. Because glycine is optically inactive, its FTC derivative is likewise expected to be inactive. The small negative signal obtained for FTC-glycine (Figure 22b) is consistent with the small negative artifact seen for fluorescein in Figure 19a. The FDCD responses for FTC-Ala, FTC-Phe, and FTC-Ser are increasingly negative and may be indicative of induced circular dichroism in the tag molecule. Since the FL signals in Figure 21 are relatively constant, these differences in FDCD signals would imply a measurable difference in FDCD/FL (i.e., a difference in optical activity). However, a second injection of FTC-Gly (Figure 22g) shows a distinct negative signal as well. This indicates that discrimination has changed between the FTC-Gly injections. Hence, the signals observed for FTC-Ala, FTC-Phe, and FTC-Ser likely contain some degree of artifact. The calculated FDCD/FL response for each amino acid is given in Table 2, but the drift in discrimination precludes the assignment of unique optical activity to these three derivatives. Drift in discrimination was confirmed by a later injection of riboflavin and fluorescein, shown in Figure 19b.

The most striking observations in these FDCD data are the increased signal magnitude and reversal of sign for FTC-Trp relative to the other

Table 2. Direct fluorescence and fluorescence-detected circular dichroism data for electrophoretic separations of FTC-amino acids shown in Figure 21 and Figure 22

Run #	Amino acid	AA conc.[a] ($\times 10^{-3}$ M)	FL[b]	FDCD[b]	FDCD/FL
a	Blank	0	--	--	--
b	Gly	1.4	+18	-4	-0.22
c	L-Ala	1.6	+12	-6.5	-0.54
d	L-Phe	1.3	+19	-17	-0.90
e	L-Ser	1.5	+15	-19	-1.3
f	L-Trp	1.4	+20	+34	+1.7
g	Gly	1.4	+18	-16	-0.89

[a]Original concentration of amino acid in the reaction mixture.

[b]FL and FDCD peak heights measured from Figures 21 and 22. Scale is arbitrary but consistent for all runs.

amino acids. Although the FL signal for the FTC-Trp peak is similar to those of the other amino acid derivatives, the FDCD signal is significantly different. The large positive signal seen for tryptophan was verified for a number of runs under different levels of discrimination. Tryptophan repeatedly gave a larger signal than the other amino acids in the set and always produced a positive signal (same sign as riboflavin). The sign of FDCD peaks for other amino acids sometimes varied. This is most likely because they are so small that any artifact (positive or negative) can overwhelm the signal. The distinct difference for FDCD of FTC-Trp has been repeatedly observed, even in old samples. In addition, on a more sensitive scale, the normalized FDCD/FL signal for FTC-L-Phe was found to be measurably different from that for FTC-Gly (data not shown).

These stronger induced FDCD signals for FTC-Trp and FTC-Phe (compared to the aliphatic amino acids tested) may be attributed to dipole-dipole interactions between the aromatic rings of the amino acids and the fluorescein tag. This possibility has been discussed by Mercola et al. (*82*) who observed induced CD in FITC isomer I bound to insulin at a Phe residue. Those authors also reported that induced CD could be measured for FITC-I when attached to an aromatic amino acid of a dipeptide (FTC-L-phenylalanyl-L-alanine), although the magnitude was much smaller than for the protein. However, they were unable to observe induced CD for FITC attached to two similar aliphatic compounds (FTC-glycyl-L-isoleucine and FTC-acetyl-L-ornithine). It appears from their CD data that the induction of optical activity into an achiral tagging

group like FITC is strongly influenced by aromaticity and rigidity within the original chiral molecule. Hiramatsu et al. (*75*) also discuss the interaction between bound FTC groups and tryptophyl residues (in lysozyme) leading to observable changes in optical activity. Therefore, the preliminary findings by FDCD presented here are consistent with CD data in the literature. The aromatic amino acids typically show larger optical rotation signals, as can be seen in Table 3. Hence, the magnitude of FDCD response (induced CD) for the FTC-amino acid derivatives appears to follow general optical activity in the amino acids.

The peaks present in the blank, though not identified, do contain some useful information. Component number 1 gives nearly uniform FL signal in each of the seven runs, but the FDCD signals associated with this peak appear to be artifacts because they are typically small and fluctuate in sign. That being the case, peak number 1 provides a means of assessing the discrimination level during this set of injections. Component number 3, on the other hand, consistently gives a large positive FDCD signal indicating optical activity. The reproducibility in FDCD/FL response for 3 (8.1% RSD) should be representative of that to be expected for other chiral analytes. No conclusions are drawn from component number 2 as the corresponding FL signals are substantially larger and show more variation than any of the other components of interest.

The comparison of FDCD signals for different FTC-amino acids is critical for the development of identification techniques based on

Table 3. Optical activity data for selected amino acids and derivatives

Amino acid	MW (g/mol)	Optical Rotation Measurements				
		Native[a]	Dansyl[b]	PTH[c] pH 5.0	FTH-I[d]	FTC-II[e]
Gly	75.05	--	-0.2	0	--	--
L-Ala	89.07	+2.7	-24	-9.4	-200	-24
L-Phe	165.10	-35.14	-224	-8.28	-1280	-490
L-Ser	105.07	-6.83	+63	-43.0	--	+43
L-Trp	204.12	-31.5	-276	≈0	+1320	-1600

[a]Specific rotation of native L-amino acids in water. Data taken from ref *88*.

[b]Specific rotation of Dansyl L-amino acid derivatives measured at 488 nm. Data taken from ref *44*.

[c]Specific rotation of phenyl thiohydantoin derivatives of L-amino acids measured at 633 nm. Data taken from ref *47*.

[d]Optical rotation data (at 350 nm) for fluorescein thiohydantoin derivatives (from FITC-I) of L-amino acids as trifluoroacetic acid salts in methanol. Data are adapted from ref *81*. The values shown here are obtained by dividing the reported [α] values by the concentrations given in g/dL.

[e]Optical rotation data (at 589 nm) for fluorescein thiocarbamyl derivatives (from FITC-II) of L-amino acids as DCHA salts in ethanol. Data are adapted from ref *80*. The values shown here are obtained by dividing the reported [α] values by the concentrations given in g/dL.

FDCD/FL. However, we are also interested in evaluating the potential of FDCD for more routine conformational analysis and determining whether it could serve as a replacement for CD and ORD when analyte concentrations fall below the detection limit for those techniques. In order to acquire some information along these lines, we compared the FDCD/FL signals for the L- and D- enantiomers of the FTC-amino acids. Typically enantiomers will exhibit mirror image CD spectra. Hence, we were interested in whether the FDCD signal would flip sign for the two isomers. These experiments were performed at higher sensitivity. The results obtained for FTC-L-Trp and FTC-D-Trp and for FTC-L-Ser and FTC-D-Ser are shown in Figure 23 and Figure 24, respectively. These samples were prepared using the same procedure described for samples in Figures 21 and 22. However, the derivatization reaction mixtures had been refrigerated for one month when these data were acquired. The migration times for the FTC-amino acids are slightly different here because a different capillary was used.

Surprisingly, both Trp enantiomers produced nearly identical FDCD/FL signals. There is no FDCD evidence of differentiation between L- and D- forms of FTC-Trp. It should be noted that the original Trp standards were verified to be of opposite handedness by CD measurements in the UV. In contrast, the FTC-Ser samples gave a distinguishable difference in FDCD sign. The FDCD signal for FTC-Ser is significantly smaller than that for FTC-Trp. (The y scale in Figure 23 is 1.4-times that in Figure 24, and the FL signals for the FTC-Ser and FTC-Trp are nearly identical.) Although the FDCD peaks for FTC-Ser are very small,

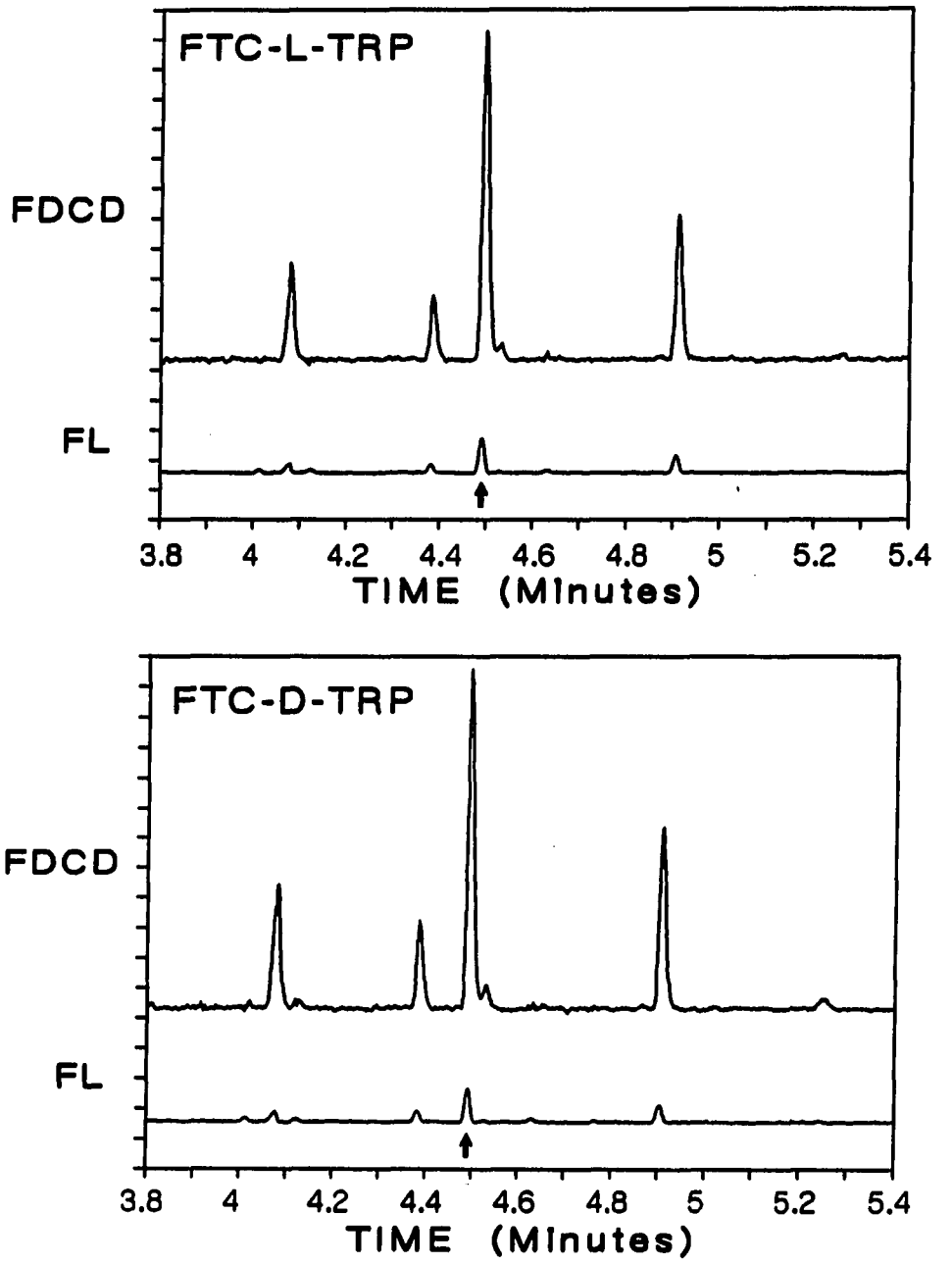

Figure 23. FDCD and FL signals obtained during capillary electrophoresis of FTC-L-tryptophan and FTC-D-tryptophan reaction mixtures
FTC-tryptophan peaks are noted by the arrow.

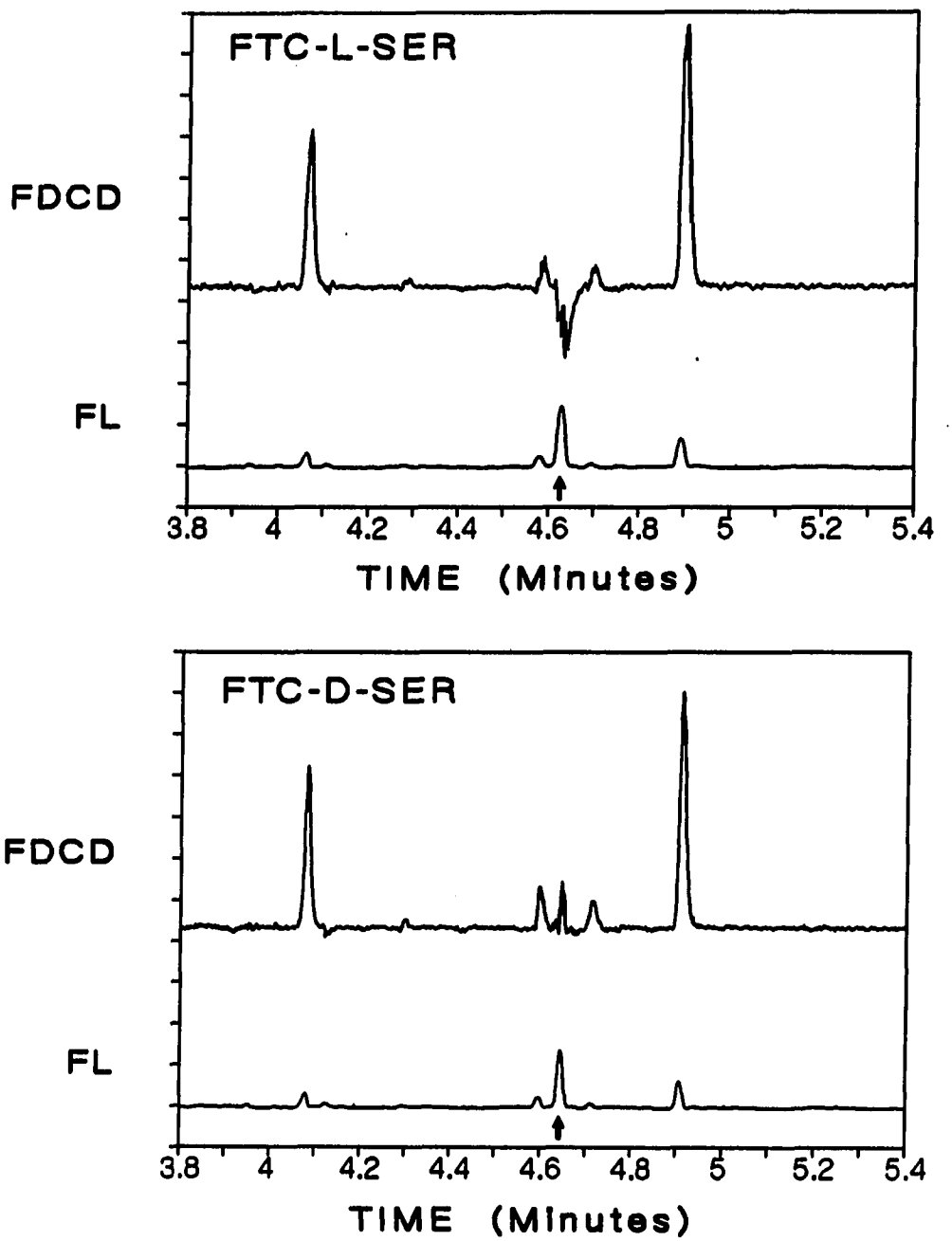

Figure 24. FDCD and FL signals obtained during capillary electrophoresis of FTC-L-serine and FTC-D-serine reaction mixtures FTC-serine peaks are noted by the arrow.

repeated injections of the Ser samples, in reversed order, gave the same results. The difference in FDCD signals for L- and D- Ser derivatives appear to be real. Further experiments are necessary to explain the unexpected behavior for L- and D- Trp derivatives. Derivatization with FITC isomer II is expected to result in a modified conformation of the derivative. FDCD/FL-CE analysis of the FITC-II derivative of Trp is one simple method which could provide insight into this issue. FDCD/FL-CE analysis on derivatives of racemic amino acids should show an absence of optical activity and could help verify the selectivity present in FDCD.

Conclusions

We have found a way to null optical artifacts, but system drift still limits quantitative capabilities. The data shown here were obtained using a 50-μm i.d. capillary. The problems of drifting are expected to be even greater when smaller capillaries are used. We have confirmed induced CD for at least some of the FTC-amino acid derivatives. The relative signal magnitudes are consistent with other optical activity data. The preliminary FDCD data for derivatized amino acids show that more improvements are necessary before the detector can be used for conclusive identification of amino acids. However we have shown that FDCD can give useful information about optical activity for less than 50 fmol of FTC-amino acids. It appears that the fluorophore does sense the chirality of the amino acid and that the effect is greatly enhanced by having an aromatic side chain on the amino acid.

Further studies are necessary to understand why no distinction was observed for the enantiomers of FTC-Trp.

CHAPTER V. FUTURE DIRECTIONS

We have demonstrated the importance of optical design in systems utilizing polarization modulation and have made substantial improvements in detectability by optimizing the modulation. In Chapter II, optimization of modulation frequency and efficiency and simplification of optical design led to a 10-fold improvement in the detectability for sodium atoms by laser polarization spectroscopy. The increased *S/N* at 150 kHz allowed operation in the dispersion mode and subsequently provided linear calibration curves. Chapters III and IV present the first studies of fluorescence-detected circular dichroism (FDCD) for on-column detection in capillary electrophoresis. Modulation efficiency and balance and preservation of desired polarization were discussed in detail and were shown to have great influence on the selectivity attainable by FDCD. Among techniques that sense optical activity, FDCD provides superior detectability on an absolute scale because it is suitable for picoliter detection volumes. Optical activity signals were observed for riboflavin (LOD = 0.2 fmol) and for less than 50 fmol of some FTC-amino acids by FDCD/FL-CE.

Limitations of these systems have also been addressed. Background noise due to stray light and laser flicker noise is minimized by the modulation and detection schemes; however, it is necessary to choose modulators and drivers that will not introduce added electronic noise. Noise-free amplification of signals requires careful selection of amplifiers also. Preservation of polarization purity is a special challenge when curved optical surfaces are present and tight focusing

is required. Technological advances in micropositioning (*89*) may prove beneficial for on-column FDCD. Improvements in mode stability and pointing stability of laser sources may be of further benefit.

Now that on-column FDCD detection has been more systematically characterized, further studies become possible. It will be necessary to widen the areas of application to develop more confidence and predictability in the method. Using visible laser sources limits the application of FDCD to those chiral fluorophores which are sensitive to visible excitation or can be derivatized to induce FDCD. UV laser sources will allow many more compounds to be studied.

A natural extension of this work is the FDCD of peptides and proteins. Circular dichroism has long been used in the study of proteins (*90, 91*), where typically, absorption bands in the far UV (below 250 nm) are studied because they provide the largest CD signal. These far-UV bands generally originate in the peptide backbone and supply information about secondary structure. A few of the common amino acids (tryptophan, phenylalanine, tyrosine, and cystine) exhibit absorption bands in the near-UV region (from 250 nm to 330 nm). The weaker CD signal originating in these near-UV bands can provide information about the tertiary structure of proteins. The challenge to better understand protein folding (*58*) is currently being pursued by several methods including CD. FDCD may offer unique structural information to help answer questions in such studies.

Development of methods for determining chiral purity is expected to increase sharply in the coming years (*92*). Because methods of

molecular design are improving, pharmaceutical compounds and related products are becoming more effective (i.e., more potent). As a result, the required dosages are decreasing, and therefore, sensitivity of analytical methods to monitor the drugs need to be improved. Since many pharmaceuticals are chiral, polarization modulation methods may play an important role in development of methods with sufficient selectivity and detectability to meet the coming challenges.

REFERENCES

1. Hecht, E. *Optics*, 2nd ed.; Addison-Wesley: Reading, MA, 1987; Chapter 8.
2. *PEM-80 Photoelastic Modulator Operation and Service Manual*, Hinds International, Inc., Hillsboro, OR; Appendix B.
3. Yeung, E. S.; Steenhoek, L. E.; Woodruff, S. D.; Kuo, J. C. *Anal. Chem.* **1980**, *52*, 1399-1402.
4. Young, M. *Optics and Lasers. Including Fibers and Optical Waveguides*, 3rd ed.; Springer-Verlag: Berlin, 1986; Chapter 8.
5. Kemp, J. C. *J. Opt. Soc. Am. A* **1969**, *59*, 950-954.
6. Andrews, D. L. *Lasers in Chemistry*; Springer-Verlag: Berlin, 1986; Chapter 3.
7. Wieman, C.; Hänsch, T. W. *Phys. Rev. Lett.* **1976**, *36*, 1170-1173.
8. Steinfeld, J. I. *Molecules and Radiation: An Introduction to Modern Molecular Spectroscopy*; MIT Press: Cambridge, MA, 1974; pp 293-295.
9. Raab, M.; Snyder, J. J. *Proc. SPIE Int. Soc. Opt. Eng.* **1983**, *426*, 99-105.
10. Wieman, C. E. *Proc. SPIE Int. Soc. Opt. Eng.* **1983**, *426*, 76-80.
11. Tong, W. G.; Yeung, E. S. *Anal. Chem.* **1985**, *57*, 70-73.
12. Lanauze, J. A.; Winefordner, J. D. *Appl. Spectrosc.* **1986**, *40*, 709-711.
13. Bobbitt, D. R.; Yeung, E. S. *Appl. Spectrosc.* **1986**, *40*, 407-410.
14. Ducloy, M.; Snyder, J. J. *Proc. SPIE Int. Soc. Opt. Eng.* **1983**, *426*, 87-90.

15. Synovec, R. E.; Yeung, E. S. *Anal. Chem.* **1985**, *57*, 2606-2610.

16. Bjorklund, G. C. *Opt. Lett.* **1980**, *5*, 15-17.

17. Teets, R. E.; Kowalski, F. V.; Hill, W. T.; Carlson, N.; Hänsch, T. W. *Proc. SPIE Int. Soc. Opt. Eng.* **1977**, *113*, 80-87.

18. Keller, J. C.; Delsart, C. *Opt. Commun.* **1977**, *20*, 147-149.

19. Ritze, H. H.; Stert, V.; Meisel, E. *Opt. Commun.* **1979**, *29*, 51-56.

20. Goldsmith, J. E. M.; Weber, E. W.; Hänsch, T. W. *Phys. Rev. Lett.* **1978**, *41*, 1525-1528.

21. Atkins, P. W. *Molecular Quantum Mechanics*, 2nd ed.; Oxford University Press: Oxford, U.K., 1983; p 212.

22. Levenson, M. D.; Eesley, G. L. *Appl. Phys.* **1979**, *19*, 1-17.

23. Zizak, G.; Lanauze, J.; Winefordner, J. D. *Appl. Opt.* **1986**, *25*, 3242-3246.

24. Raab, M.; Weber, A. *J. Opt. Soc. Am. B* **1985**, *2*, 1476-1479.

25. Synovec, R. E.; Yeung, E. S. *J. Chromatogr.* **1986**, *368*, 85-93.

26. Davis, L. A.; Krupa, R. J.; Winefordner, J. D. *Spectrochim. Acta, Part B* **1986**, *41*, 1167-1174.

27. Borman, S. *Anal. Chem.* **1987**, *59*, 969A-973A.

28. Smith, L. M. *Anal. Chem.* **1988**, *60*, 381A-390A.

29. Garnick, R. L.; Solli, N. J.; Papa, P. A. *Anal. Chem.* **1988**, *60*, 2546-2557.

30. Jinno, K.; Fujimoto, C. *LC-GC* **1989**, *7*, 328-338.

31. Novotny, M. V. *Science* **1989**, *246*, 51-57.

32. Kennedy, R. T.; Oates, M. D.; Cooper, B. R.; Nickerson, B.; Jorgenson, J. W. *Science* **1989**, *246*, 57-63.

33. Mikkers, F. E. P.; Everaerts, F. M.; Verheggen, Th. P. E. M. *J. Chromatogr.* **1979**, *169*, 11-20.

34. Huang, X.; Pang, T. J.; Gordon, M. J.; Zare, R. N. *Anal. Chem.* **1987**, *59*, 2747-2749.

35. Kuhr, W. G.; Yeung, E. S. *Anal. Chem.* **1988**, *60*, 1832-1834.

36. Kuhr, W. G.; Yeung, E. S. *Anal. Chem.* **1988**, *60*, 2642-2646.

37. Turner, D. H.; Tinoco, I, Jr.; Maestre, M. *J. Am. Chem. Soc.* **1974**, *96*, 4340-4342.

38. Tinoco, I., Jr.; Turner, D. H. *J. Am. Chem. Soc.* **1976**, *98*, 6453-6456.

39. Lobenstine, E. W.; Turner, D. H. *J. Am. Chem. Soc.* **1980**, *102*, 7786-7787.

40. Kuo, J. C.; Yeung, E. S. *J. Chromatogr.* **1981**, *223*, 321-329.

41. Kuo, J. C.; Yeung, E. S. *J. Chromatogr.* **1982**, *229*, 293-300.

42. Kuo, J. C.; Yeung, E. S. *J. Chromatogr.* **1982**, *253*, 199-204.

43. Reitsma, B. H.; Yeung, E. S. *J. Chromatogr.* **1986**, *362*, 353-362.

44. Reitsma, B. H.; Yeung, E. S. *Anal. Chem.* **1987**, *59*, 1059-1061.

45. Reitsma, B. H.; Yeung, E. S. *J. Chromatogr.* **1987**, *405*, 295-303.

46. Bobbitt, D. R.; Yeung, E. S. *Anal. Chem.* **1984**, *56*, 1577-1581.

47. Chan, K. C.; Yeung, E. S. *J. Chromatogr.* **1988**, *457*, 421-426.

48. Boehme, W.; Wagner, G.; Oehme, U.; Priesnitz, U. *Anal. Chem.* **1982**, *54*, 709-711.

49. Cheng, Y. F.; Dovichi, N. J. *Science* **1988**, *242*, 562-564.

50. Lobenstine, E. W.; Turner, D. H. *J. Am. Chem. Soc.* **1979**, *101*, 2205-2207.

51. Turner, D. H.; Tinoco, I, Jr.; Maestre, M. F. *Biochemistry* **1975**, *14*, 3794-3799.

52. Jorgenson, J. W.; Lukacs, K. D. *Anal. Chem.* **1981**, *53*, 1298-1302.

53. Jorgenson, J. W.; Lukacs, K. D. *Science* **1983**, *222*, 266-272.

54. Jorgenson, J. W. *Anal. Chem.* **1986**, *58*, 743A-760A.

55. Gordon, M. J.; Huang, X.; Pentoney, S. L., Jr.; Zare, R. N. *Science* **1988**, *242*, 224-228.

56. Ewing, A. G.; Wallingford, R. A.; Olefirowicz, T. M. *Anal. Chem.* **1989**, *61*, 292A-303A.

57. Smith, L. M.; Sanders, J. Z.; Kaiser, R. J.; Hughes, P.; Dodd, C.; Connell, C. R.; Heiner, C.; Kent, S. B. H.; Hood, L. E. *Nature* **1986**, *321*, 674-679.

58. King, J. *Chem. Eng. News* **1989**, *67*(15), 32-54.

59. Neuhoff, V. *Electrophoresis* **1984**, *5*, 251.

60. Radola, B. J. *Electrophoresis* **1980**, *1*, 43-56.

61. Christensen, P. L.; Yeung, E. S. *Talanta* **1989**, *36*, 179-184.

62. Folestad, S.; Johnson, L.; Josefsson, B.; Galle, B. *Anal. Chem.* **1982**, *54*, 925-929.

63. McCormick, R. M. *Anal. Chem.* **1988**, *60*, 2322-2328.

64. Lukacs, K. D.; Jorgenson, J. W. *J. HRC CC, J. High Resolut. Chromatogr. Chromatogr. Commun.* **1985**, *8*, 407-411.

65. Nickerson, B.; Jorgenson, J. W. *HRC CC, J. High Resolut. Chromatogr. Chromatogr. Commun.* **1988**, *11*, 533-534.

66. Gassmann, E.; Kuo, J. E.; Zare, R. N. *Science* **1985**, *230*, 813-814.

67. Gozel, P.; Gassmann, E.; Michelsen, H.; Zare, R. N. *Anal. Chem.* **1987**, *59*, 44-49.

68. Lehninger, A. L. *Principles of Biochemistry*; Worth Publishers, Inc.: New York, NY, 1982; Chapter 6.

69. Schlesinger, D. H. In *CRC Handbook of HPLC for the Separation of Amino Acids, Peptides, and Proteins*; Hancock, W. S., Ed.; CRC Press: Boca Raton, FL, 1984; Vol. I, pp 367-379.

70. Bhown, A. S.; Bennett, J. C. In *CRC Handbook of HPLC for the Separation of Amino Acids, Peptides, and Proteins*; Hancock, W. S., Ed.; CRC Press: Boca Raton, FL, 1984; Vol. II, pp 267-278.

71. Christensen, P. L.; Yeung, E. S. *Anal. Chem.* **1989**, *61*, 1344-1347.

72. Green, S. C.; Jorgenson, J. W. *HRC CC J. High Resolut. Chromatogr. Chromatogr. Commun.* **1984**, *7*, 529-531.

73. Seiler, N.; Demisch, L. In *Handbook of Derivatives for Chromatography*; Blau, K.; King, G. S., Eds.; Heyden: London, U.K., 1977; Chapter 9.

74. Knapp, D. R. *Handbook of Analytical Derivatization Reactions*; John Wiley and Sons: New York, NY, 1979; pp 274-287.

75. Hiramatsu, M.; Okabe, N.; Tomita, K. *J. Biochem.* **1973**, *73*, 971-978.

76. Postnikova, G. B.; Yumakova, E. M.; Sukhomudrenko, A. G.; Volkenshtein, M. V.; Atanasov, B. P. *Biophys. Chem.* **1980**, *11*, 29-37.

77. Halfman, C. J.; Dowe, R.; Jay, D. W.; Schneider, A. S. *Molec. Immun.* **1986**, *23*, 943-949.

78. Burtnick, L. D. *Biochim. Biophys. Acta* **1984**, *791*, 57-62.

79. Velluz, L.; Legrand, M.; Grosjean, M. *Optical Circular Dichroism. Principles, Measurements, and Applications*; MacCordick, J., Transl.; Academic Press: New York, NY, 1965; Chapter 3.

80. Kawauchi, H.; Kadooka, K.; Tanaka, M.; Tuzimura, K. *Agric. Biol. Chem.* **1971**, *35*, 1720-1726.

81. Kawauchi, H.; Tuzimura, K. *Agric. Biol. Chem.* **1971**, *35*, 150-157.

82. Mercola, D. A.; Morris, J. W. S.; Arquilla, E. R. *Biochemistry* **1972**, *11*, 3860-3874.

83. Kaufman, G. I.; Nester, J. F.; Wasserman, D. E. *J. Histochem. Cytochem.* **1971**, *19*, 469-476.

84. Einarsson, S.; Josefsson, B.; Möller, P.; Sanchez, D. *Anal. Chem.* **1987**, *59*, 1191-1195.

85. Tsubokawa, M.; Kawauchi, H.; Li, C. H. *J. Biochem.* **1980**, *88*, 1407-1412.

86. Muramoto, K.; Kamiya, H.; Kawauchi, H. *Anal. Biochem.* **1984**, *141*, 446-450.

87. Kawauchi, H.; Tuzimura, K.; Maeda, H.; Ishida, N. *J. Biochem.* **1969**, *66*, 783-789.

88. *CRC Handbook of Chemistry and Physics*, 63rd Ed.; Weast, R. C., Ed.; CRC Press: Boca Raton, FL, 1982; p C-757.

89. Belleville, L. *Laser Focus World* **1990**, *26*, 113-129.

90. Strickland, E. H. *CRC Crit. Rev. Biochem.* **1974**, *2*, 113-175.

91. Cantor, C. R.; Schimmel, P. R. *Biophysical Chemistry. Part II: Techniques for the Study of Biological Structure and Function*; W. H. Freeman: New York, 1980; Chapter 8.

92. Borman, S. *Chem. Eng. News* **1990**, *68*(28), 9-14.

ACKNOWLEDGMENTS

Many are deserving of acknowledgment at the completion of this work. I express thanks to Professor Edward Yeung for allowing me the opportunity to do graduate research in the field of laser polarization spectroscopy and for widening my perception of science. To my former teachers and mentors in scientific and nonscientific disciplines, I express thanks for the encouragement and inspiration given throughout my formal education. The support and fellowship of family and friends have always been essential factors in my accomplishments, and I thank each of them for helping me keep the necessary balance in my life. Finally, for the special joy he brings, his unending love and support, and his commendable patience, I am forever grateful to my proofreader, Kevin.

This work was performed at Ames Laboratory under contract no. W-7405-eng-82 with the U. S. Department of Energy. The United States government has assigned the DOE Report number IS-T 1449 to this thesis.